



Article

Operational Optimization of Seasonal Ice-Storage Systems with Time-Series Aggregation

Maximilian Hillen ^{1,2,*} , Patrik Schönfeldt ³ , Philip Groesdonk ¹ and Bernhard Hoffschmidt ^{1,2}

¹ German Aerospace Center (DLR), Institute of Solar Research, 52428 Juelich, Germany; philip.groesdonk@dlr.de (P.G.); bernhard.hoffschmidt@dlr.de (B.H.)

² Faculty of Mechanical Engineering, RWTH Aachen University, Chair of Solar Components, 51147 Cologne, Germany

³ German Aerospace Center (DLR), Institute of Networked Energy Systems, 26129 Oldenburg, Germany; patrik.schoenfeldt@dlr.de

* Correspondence: maximilian.hillen@dlr.de

Abstract

The transition to sustainable energy systems increasingly relies on advanced optimization methods to address the challenges of designing and operating them efficiently. Seasonal storage systems play a pivotal role in aligning renewable energy generation with fluctuating energy demand, with ice storage emerging as a promising solution for seasonal energy storage. This paper presents a novel optimization framework for the operation of seasonal ice-storage systems, leveraging Mixed-Integer Linear Programming (MILP) with time-series aggregation (TSA) techniques. The proposed model accurately captures the physical behavior of ice storage, incorporating both latent and sensible heat storage phases, discrete temperature levels, and charging/discharging efficiency curves. A key feature of this framework is its ability to address computational challenges in large-scale optimization, while maintaining high detail. Using a business park in Germany as a case study, the results demonstrate a significant reduction in computational time of up to 80% for 110 typical periods, with only a 2.5% deviation in the objective value and 9% in the Seasonal Energy Efficiency Ratio (SEER), although this efficiency gain depends on the number of typical periods used. This work addresses key gaps in seasonal ice-storage optimization models and provides a robust tool for designing and optimizing sustainable energy systems.



Academic Editor: Antonio Rosato

Received: 14 October 2025

Revised: 6 November 2025

Accepted: 11 November 2025

Published: 14 November 2025

Citation: Hillen, M.; Schönfeldt, P.; Groesdonk, P.; Hoffschmidt, B. Operational Optimization of Seasonal Ice-Storage Systems with Time-Series Aggregation. *Energies* **2025**, *18*, 5988. <https://doi.org/10.3390/en18225988>

Copyright: © 2025 by the authors. Licensee MDPI, Basel, Switzerland. This article is an open access article distributed under the terms and conditions of the Creative Commons Attribution (CC BY) license (<https://creativecommons.org/licenses/by/4.0/>).

Keywords: seasonal storage; ice storage; MILP; time-series aggregation; energy system optimization

1. Introduction

The increasing reliance on renewable energy sources introduces significant challenges in balancing energy supply and demand, both on daily (day–night) and seasonal (summer–winter) timescales. This mismatch is particularly pronounced because renewable energy generation, such as solar and wind, is not only variable and intermittent but its fluctuations also align with distinct daily and seasonal patterns [1]. Thermal energy storage (TES) offers a promising solution by decoupling energy generation from consumption, providing a buffer to store excess thermal energy for later use in heating and cooling applications [2]. TES systems are categorized into three main types: sensible heat, latent heat, and thermochemical storage. In sensible heat storage, energy is stored by changing the temperature of a medium, while latent heat storage utilizes phase changes (e.g., from solid to liquid). Thermochemical storage depends on the reversible chemical reactions of a material [3,4].

TES technologies are at different maturity levels: sensible heat storage is already commercial at scale, while latent-heat and thermochemical storage are progressing from field trials and pilot demonstrations toward broader deployment as materials, integration methods, and standards mature [5–11]. Latent heat storage, particularly systems based on Phase Change Materials (PCMs), such as water/ice, salt hydrates and paraffin waxes, has a high potential due to its superior energy density. However, such systems often carry higher risks, such as material toxicity and cost concerns [12]. Among various PCM, water/ice stands out as the most cost-effective and environmentally friendly option, offering economic advantages over alternatives such as eutectic salts, polyethylene glycol, and paraffin [13].

Optimization plays a pivotal role in the effective planning and operation of energy systems, enabling improved performance, cost reduction, and sustainable resource management [14]. Despite the advantages of ice-storage systems, challenges persist in optimizing their seasonal operation, particularly when accounting for the seasonal variability in thermal energy demand and the interplay of various energy system components. Many existing models significantly simplify their frameworks to reduce computational time, which can lead to less accurate representations of system dynamics [15]. The focus of this paper is to address these challenges by proposing an operational cost-optimization modeling framework using time-series aggregation (TSA) for seasonal operation, applicable to both monitoring and planning.

1.1. Operational Modeling of Ice Storage: Literature Review

Ice-storage systems operate either on a daily or a seasonal basis. In daily systems, ice is produced at night and discharged during the day to compensate for peaks in demand, which is typically cost effective in climates with high temperature fluctuations between day and night [16–20]. Seasonal systems use a heat pump in winter to extract and freeze the ice storage and then provide cooling from the tank in summer; these are generally advantageous where winters are cold and summers require cooling [21–24].

The freezing and melting of ice are analytically and numerically challenging due to these phase transitions involving not only a change between mediums with distinct thermal properties but also the release or absorption of latent heat of fusion [17].

Existing operational models range from rule-based to advanced optimization and differ in key factors such as phase transitions, ice-level-dependent charge/discharge effectiveness, and temperature levels of energy flows, which determine, for example, the heat-pump Coefficient of Performance (COP) of the ice storage.

The models are summarized in Table 1 for a comprehensive comparison and are categorized by their operational modeling, the so-called key factors, as well as time horizons and resolution. The citations in the following review follow the same order as in the table, beginning with rule-based approaches and progressing to long-term optimization models.

Physics-based simulation captures freezing/melting and temperature fields with high fidelity, two-phase flow models to validate transient heat-transfer formulations [8,17,25–27]. These studies resolve phase transitions and temperature levels for daily and seasonal patterns but do not optimize the operation.

Control- and data-driven methods (rule-based, Model Predictive Control (MPC) or system identification) primarily target short-horizon operational savings, often under time-varying tariffs [28–31]. Most omit explicit temperature levels and only partly capture charging/discharging effectiveness; [9,21] are the only studies using seasonal data, but their identified relations are not embedded in a seasonal, physics-consistent optimization.

Cost-optimal operation with optimization models uses Dynamic Programming (DP), Evolutionary Algorithm (EA), Mixed-Integer Linear Programming (MILP), Mixed-Integer Quadratic Programming (MIQP), or Mixed-Integer Nonlinear Programming (MINLP) over

daily horizons and commonly omits explicit two-phase dynamics; some include linearized effectiveness curves or fix performance at a nominal state [18–20,32–38]. These formulations scale well but risk bias when seasonal storage patterns matter.

Heine et al. present the only seasonal MILP; they fix performance at a nominal state and omit explicit phase change and temperature levels—scalable over a full year but not physics consistent for hourly detail [36]. Vivian et al. tackle a seasonal, quadratically constrained MINLP with two storage phases but without effectiveness curves; the 8 h time step sacrifices daily peaks and short-cycle dynamics [23]. Odufuwa et al. span a long horizon via MINLP switching but model storage as single-phase with fixed COP relations—no latent heat or temperature-level modeling [39].

Table 1. Modeling references for operational modeling and optimization studies.

| Source | Operational Modeling | | | | | | | Liquid and Frozen Phase | Effect-iveness Curves | Variable Temperature Levels | Time in Hours | |
|-----------|----------------------|-----|----|--------------|------|------|-------|-------------------------|-----------------------|-----------------------------|---------------|------------|
| | Rule Based | | | Optimization | | | | | | | Horizon | Resolution |
| | Simulation | MPC | DP | EA | MILP | MIQP | MINLP | | | | | |
| [17] | x | | | | | | | x | | x | 24 | 30/60 |
| [25] | x | | | | | | | x | x | | 24 | 1/60 |
| [8] | x | | | | | | | x | x | x | 24 | 1/60 |
| [26] | x | | | | | | | x | x | x | 8760 | 1 |
| [27] | x | | | | | | | x | x | x | 8760 | 1 |
| [21] | x | x | | | | | | | | | 8760 | 1 |
| [28] | x | x | | | | | | x | | | 24 | 1 |
| [29] | x | x | x | | | | | | | | 24 | 1 |
| [30] | x | | x | | | | | | x | x | 24 | 1 |
| [31] | | x | | | | | | x | x | | 24 | 5/60 |
| [9] | | x | | | | | | | | x | 8760 | 1 |
| [34] | | x | | | x | | | | | | 24 | 15/60 |
| [40] | | | | x | | | | | | | 24 | 1 |
| [37] | | | | | x | | | | | | 24 | 1 |
| [19] | | | x | | | | | | x | | 24 | 1 |
| [32] | | | | | x | | | | | | 24 | 1 |
| [18] | | | | | x | | | | | | 24 | 1 |
| [38] | | | | | x | | | | | | 24 | 1 |
| [35] | | | | | x | | | | x | | 24 | 1 |
| [41] | | | | | x | | | | | x | 24 | 1 |
| [13] | | | | | | x | | x | | x | 24 | 30/60 |
| [20] | | | | | x | | | x | | | 24 | 1 |
| [33] | | | | | x | | | | | x | 48 | 5/60 |
| [42] | | | | | | | x | | | | 24 | 1 |
| [39] | | | | | | | x | | | x | 2880 | 1 |
| [36] | | | | | x | | | | | | 8760 | 15/60 |
| [23] | | | | | | | x | x | | | 8760 | 8 |
| This work | | | | | x | | | x | x | x | 8760 | 1 |

1.2. Optimization of Seasonal Storage by Considering Aggregated Time-Series

TSA reduces the number of time steps while preserving key dynamics by clustering or otherwise compressing recurring patterns (e.g., typical days or weeks) in demands and renewable energy source capacities [43]. In energy-system models, each typical period represents a distinct operational time frame whose contribution is scaled by its frequency in the original series. This scaling can be performed as a weighting in the cost function. For clustering-based aggregation, this impact is determined by the cardinality of the cluster

represented by the period. The sequence of periods in the original time-series is not considered in this process [44].

To cut computation while retaining seasonal dynamics, prior work varies temporal granularity across components—using longer time steps for long-term storage and shorter time steps elsewhere—with limited accuracy loss [45]. Sequence-aware formulations couple typical periods via storage balance written on the original layer while other constraints use aggregated periods [46]. A unified approach models storage with inter-period (links between typical periods) and intra-period (within a period) states on these two time layers without the original time layer, enabling the linear operational optimization of seasonal storage with typical periods [44].

1.3. Chosen Model Template as Optimization Framework

MILP is widely used in the storage optimization process as discussed in Section 1.1. However, its application to heat supply systems is limited because the energy flow in these systems depends on both the mass flow and the temperature, which makes the optimization problem quadratic. To simplify, many models do not explicitly consider temperature levels.

Model Template for Residential Energy Supply Systems (MTRESS), an open-source implementation that wraps the open energy modeling framework (oemof) [47], addresses this problem. It consists of five main classes: *Energy System*, *Location*, *Energy Carrier*, *Component*, and *Demand*. MTRESS simplifies the creation of energy systems by eliminating the need for users to manually set connections [48]. In addition, it incorporates discrete temperature levels. This approach enables the calculation of efficiencies for heating technologies with temperature-dependent efficiencies, such as heat pumps or solar thermal plants, providing a more accurate representation of reality. Moreover, heat storage systems are modeled with sub-volumes for each temperature level, allowing for temperature-dependent loading, unloading, and losses. The heat demands are represented by a reduction in the temperature of the flow, which allows a detailed and realistic simulation of the heat supply systems [49].

1.4. Research Gap and Contribution

Existing models for seasonal operational optimization of ice storage within multi-carrier energy systems have notable limitations, primarily imposed by computational tractability, that reduce their effectiveness and accuracy in representing real-world operation (as shown in Table 1). These limitations are outlined as follows:

- Variable temperature levels and phase states: Many ice-storage optimization models neglect the two-phase (ice/water) behavior and the temperature levels of both the sensible portion of the storage and the system's heat flows. Our model couples the storage phase state and temperature levels—both in the tank and in the heat flows—capturing temperature-driven performance (e.g., the heat-pump COP) endogenously.
- Charge/discharge effectiveness: Existing formulations in seasonal optimization omit the state-dependent effectiveness of charging/discharging. We add effectiveness curves as functions of the ice level into the optimization model and linearize them to enhance performance realism, while explicitly analyzing the resulting impact on computational effort.
- Physics with annual horizon and fine operation: Current optimization approaches trade annual horizons for coarse time steps (or vice versa), missing phase-change dynamics and daily peaks. We preserve physical ice behavior over a yearly horizon using TSA with inter-/intra-period storage states, enabling seasonal operational optimization with sub-daily fidelity.

By addressing these limitations, this paper presents a seasonal operational optimization approach, formulated as a MILP, that more accurately captures the physical behavior

of ice storage compared to prior models. To maintain computational efficiency, we apply TSA for seasonal storage. Unlike recent studies with TSA, our approach models the storage system in greater physical detail. Additionally, we extend the standard two-layer inter-/intra-period formulation by introducing a third time layer with selected binary state variables to represent the storage phase state. This extension preserves temperature- and COP-dependent behavior under aggregation, and we systematically investigate the influence of the additional time layer on performance metrics and technical performance indicators.

2. Methods

This section outlines the modeling approach and operational constraints utilized to optimize the performance of seasonal ice-storage systems. First, we describe the physics of ice storage in Section 2.1. Next, we derive the operational constraints in Section 2.2, which encompass the performance of the ice storage and the ice-storage heat pump, as well as the charging and discharging constraints, their effectiveness, and discrete temperature levels. Finally, in Section 2.3, we introduce TSA techniques and discuss their limitations in applying optimization to ice-storage systems and how we overcome these challenges.

2.1. Ice-Storage Physics

It is assumed that the water in the ice-storage tank st is ideally mixed and that the ice-storage tank is cylindrical like the models implemented by Viessmann [50]. The volume of storage V_{st} is calculated using Equation (1), which takes the storage height h_{st} and diameter d_{st} :

$$V_{st} = \pi \cdot h_{st} \cdot (d_{st}/2)^2 \quad (1)$$

The storage capacity for fully frozen storage $Q_{st,frz}^{\max}$ is equal to the product of the storage volume V_{st} , the melting enthalpy h_f and the density of ice ρ_{ice} (Equation (2)),

$$Q_{st,frz}^{\max} = V_{st} \cdot \rho_{ice} \cdot h_f \quad (2)$$

while the storage capacity for the liquid phase $Q_{st,liq}^{\max}$ is calculated as shown in Equation (3), with the product of the subtraction of the maximum storage temperature T_{st}^{\max} and the melting temperature of ice T_{melt} , simplified for tractability and as a conservative lower bound with 0 °C, the density of water ρ_{water} and the storage volume V_{st} :

$$Q_{st,liq}^{\max} = V_{st} \cdot \rho_{water} \cdot c_{p,water} \cdot (T_{st}^{\max} - T_{melting}) \quad (3)$$

The maximum storage capacity Q_{st}^{\max} is the sum of the liquid and frozen capacity (Equation (4)):

$$Q_{st}^{\max} = Q_{st,liq}^{\max} + Q_{st,frz}^{\max} \quad (4)$$

Heat exchange between ice storage and the ground is, as in other assumed models, limited to the cylindrical part of the ice and the base plate [22]. With this surface area of the storage tank $A_{st,surface}$, determined in Equation (5),

$$A_{st,surface} = \pi \cdot (d_{st}/2)^2 + \pi \cdot d_{st} \cdot h_{st} \quad (5)$$

the heat transfer coefficient U_{st} , the external temperature of the ground T_{grd} , and the storage temperature T_{st} , the thermal loss of the storage $Q_{st,loss}$ can be calculated with Equation (6):

$$Q_{st,loss} = U_{st} \cdot A_{st,surface} \cdot (T_{st} - T_{grd}) \quad (6)$$

The actual ice-storage content Q_{st} can be calculated by using Equation (2), which represents the latent part, with the ice level X_{st} in the range of $0 \leq X_{st} \leq 1$, where $X_{st} = 0$ indicates no ice and $X_{st} = 1$ indicates fully frozen, and Equation (3), which represents the sensible part, with the storage temperature T_{st} as shown in Equation (7):

$$Q_{st} = V_{st} \cdot (\rho_{\text{water}} \cdot c_{p,\text{water}} \cdot (T_{st}^{\max} - T_{st}) + \rho_{\text{ice}} \cdot h_f \cdot X_{st}) \quad (7)$$

For this, the technical limitations of an ice storage can be established by a maximum ice level X_{st}^{\max} and the maximum storage temperature T_{st}^{\max} .

2.2. Operation Constraints

We use the *GenericStorage* component from oemof, which models a storage system with configurable input/output flows, efficiency, and loss rates. For each time step t the input flow $\dot{Q}_{st,t}^{\text{in}}$ represents the energy entering the storage, while the output flow $\dot{Q}_{st,t}^{\text{out}}$ represents the energy discharged. Each flow is subject to efficiency factors for charging $\eta_{st,t}^{\text{in}}$ and for discharging $\eta_{st,t}^{\text{out}}$, while $\delta_{st,t}$ represents absolute losses. We simplify the storage content constraint to Equation (8):

$$Q_{st,t+1} = Q_{st,t} - \delta_{st,t} - \frac{\dot{Q}_{st,t}^{\text{out}}}{\eta_{st,t}^{\text{out}}} + \dot{Q}_{st,t}^{\text{in}} \cdot \eta_{st,t}^{\text{in}} \quad (8)$$

Vivian et al. introduced a state variable, in the form of a binary variable varying over time, to model whether storage is in a melting phase or a liquid phase [23]. This binary variable $s_{st,t}$ defines if $s_{st,t} = 1$ such that the storage is in a melting phase, while $s_{st,t} = 0$ applies to the liquid phase. The state variable is modeled by a big-m method with $M \geq 1$ (Equation (9)):

$$\begin{aligned} \frac{Q_{st,\text{liq}}^{\max}}{Q_{st}^{\max}} &\geq \frac{Q_{st,t+1}}{Q_{st}^{\max}} - M \cdot s_{st,t} \\ \frac{Q_{st,\text{liq}}^{\max}}{Q_{st}^{\max}} &\leq \frac{Q_{st,t+1}}{Q_{st}^{\max}} + M \cdot (1 - s_{st,t}) \end{aligned} \quad (9)$$

2.2.1. Heat Carrier for Variable Temperature Levels

Schönfeldt et al. introduced discrete temperature levels for heating flows in the optimization of linear problems in MTRESS [48]. Assuming that the density, volume flow, and thermal capacity of the fluid in both the heating and cooling circuits are constant and temperature dependent, the temperature significantly affects the efficiency of components such as heat pumps, as well as the thermal losses in storage systems. Therefore, incorporating temperature into the optimization process is a logical step. In this context, we use m discrete temperature levels for heating, and since cooling flows were not previously included, extend the formulation to n discrete temperature levels for cooling.

The following equations describe the relationship between these discrete temperature levels for both heating and cooling processes:

$$\begin{aligned} T_{m+1} &> T_m \geq \min(T_m) \\ T_{n+1} &< T_n \leq \max(T_n) \end{aligned} \quad (10)$$

We assume that the temperature of a heating flow can always be reduced and that, for cooling, it can always be increased. Thus, any heat source that supplies thermal energy at T_m can supply at least the same amount at T_{m-1} , and any cooling source that supplies thermal energy at T_n can supply at least the same amount of cooling at T_{n-1} .

Moreover, heat can be gradually transferred from a lower level T_m to a higher level T_{m+1} . To do so, for example, heat entering the heat supply system $\dot{Q}_{m+1,t}^{\text{in}}$ supplied by a heating technology at the temperature level T_m is composed of heat from the next lower level $\dot{Q}_{m,t}^{\text{in}}$ at the temperature level T_m and is expressed in

$$\dot{Q}_{m+1,t}^{\text{in}} = (1 - r_{m+1,m}) \cdot \dot{Q}_{m,t}^{\text{out}} + r_{m+1,m} \cdot \dot{Q}_{m+1,t}^{\text{in}}, \quad (11)$$

where $r_{m+1,m}$ represents the energy reduction factor between temperature levels T_{m+1} and T_m as calculated by

$$r_{m+1,m} = \frac{T_{m+1} - T_m}{T_{m+1} - \min(T_m)}, \quad (12)$$

which serves as a multiplication factor for the energy at the lower temperature level T_m and guarantees that heat cannot be transferred from a lower to a higher level without applying external work.

In our model, each thermal demand d that is used for heating $Q_{d,m+1,t}$ has a flow T_{m+1} and return temperature T_m . In this example, the flow temperature is the next higher temperature level $m+1$ but can be any higher temperature level. A heating demand is a reduction in temperature and is modeled analogously to Equation (11) by

$$\dot{Q}_{m,t}^{\text{out}} = (1 - r_{m+1,m}) \cdot \dot{Q}_{d,m+1,t} + r_{m+1,m} \cdot \dot{Q}_{m+1,t}^{\text{in}}, \quad (13)$$

Figure 1 illustrates the relationship between the discrete temperature levels for heating flows, demand, and the necessary reduction factors.

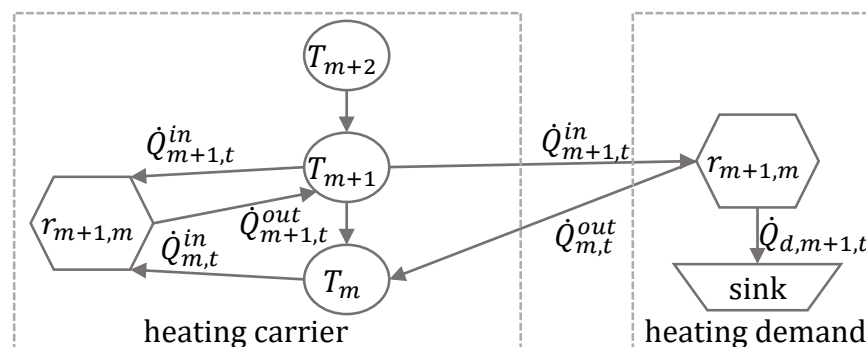


Figure 1. Flow chart with temperature levels for heating carrier and heating demand.

For cooling, the logic is the same but vice versa. Meanwhile, cooling can be transferred from a higher level to a lower level but with an increase in thermal energy, using the energy-raising factor $r_{n,n+1}$ shown in Equation (14):

$$r_{n,n+1} = \frac{T_n - T_{n+1}}{\max(T_n) - T_n}, \quad (14)$$

Following this, cooling energy can be gradually transferred from a higher to a lower level by

$$\dot{Q}_{n,t}^{\text{in}} = (1 - r_{n,n+1}) \cdot \dot{Q}_{n+1,t}^{\text{out}} + r_{n,n+1} \cdot \dot{Q}_{n,t}^{\text{in}}, \quad (15)$$

with the cooling demand modeled by

$$\dot{Q}_{n+1,t}^{\text{out}} = (1 - r_{n,n+1}) \cdot \dot{Q}_{d,n,t} + r_{n,n+1} \cdot \dot{Q}_{n,t}^{\text{in}}. \quad (16)$$

2.2.2. Ice-Storage Constraint for Discrete Temperature Levels

In this work, the constraints of the ice storage are formulated such that the cooling energy is represented with a positive sign. This implies that when the storage tank is fully frozen, it has reached its maximum storage capacity. Discrete temperature levels are incorporated into the storage model as the available potential for charging and discharging depends on the current storage temperature.

Assuming that the lowest temperature level of the ice storage corresponds to the phase change temperature of 0 °C, the storage content for the levels of heat carrier cooling temperature n above the phase change temperature can be expressed as a parameter by simplifying Equation (7) to Equation (17):

$$Q_{st,n,t} = V_{st} \cdot \rho_{\text{water}} \cdot c_{p,\text{water}} \cdot (T_{st}^{\max} - T_{n,t}) \quad (17)$$

The binary variable $o_{st,n,t}$ indicates whether discharging is possible at the temperature level n during time t ; if $o_{st,n,t} = 1$, discharging is allowed, and if $o_{st,n,t} = 0$, it is not. The binary variable $i_{st,n,t}$ indicates the feasibility of charging; if $i_{st,n,t} = 0$ it is possible, and if $i_{st,n,t} = 1$ it is not. These conditions are formulated in Equation (18):

$$\begin{aligned} \frac{Q_{st,t+1}}{Q_{st}^{\max}} &\geq o_{st,n,t} \cdot \frac{Q_{st,n}}{Q_{st}^{\max}} \\ \frac{Q_{st,t+1}}{Q_{st}^{\max}} &\leq i_{st,n,t} + \frac{Q_{st,n}}{Q_{st}^{\max}} \end{aligned} \quad (18)$$

The distinction between charging and discharging arises from the assumption that charging is always possible at temperatures at or below the phase change temperature of 0, °C. This reflects that ice storage can charge at these temperatures, but discharging is not possible below 0, °C, as the ice cannot cool further in our model. Figure 2 illustrates the charging and discharging of the ice-storage model for different temperature levels.

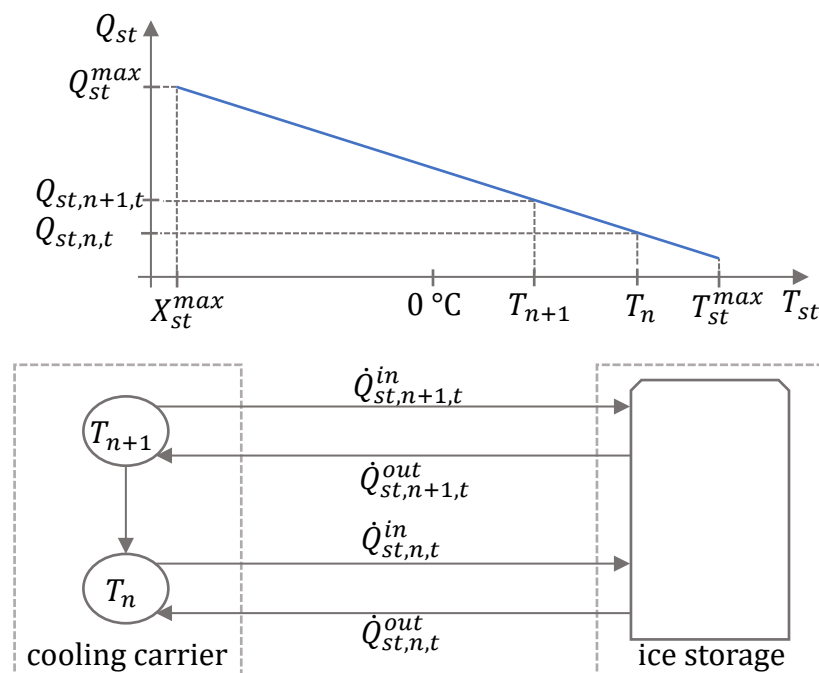


Figure 2. The relationship between the ice-storage content and its ice level for discrete temperature levels, and the resulting inflows and outflows.

Furthermore, with binary variables $o_{st,n,t}$ and $i_{st,n,t}$, along with the maximum charging and discharging rates $\dot{Q}_{st}^{\text{in,max}}$ and $\dot{Q}_{st}^{\text{out,max}}$, the actual charging power $\dot{Q}_{st,n,t}^{\text{in}}$ and discharging power $\dot{Q}_{st,n,t}^{\text{out}}$ for each discrete temperature level can be constrained as shown in Equation (19):

$$\begin{aligned}\frac{\dot{Q}_{st,n,t}^{\text{out}}}{\dot{Q}_{st}^{\text{out,max}}} &\leq o_{st,n,t} \\ \frac{\dot{Q}_{st,n,t}^{\text{in}}}{\dot{Q}_{st}^{\text{in,max}}} &\leq 1 - i_{st,n,t}\end{aligned}\quad (19)$$

2.2.3. Ice-Storage Heat Pump Model for Discrete Temperature Levels

The model of the heat pump connected to the ice storage is defined for each ice-storage heat pump, denoted hp_ice , and for discrete ice-storage temperature levels l . Since the ice-storage heat pump uses the ice storage as an exergy source, it is crucial to model this interaction with temperature levels. For each source temperature level l of the ice storage, and for each heat carrier temperature level m , an individual COP is calculated.

For this, for each temperature level l , a binary variable $o_{st, hp_ice, l, t}$ is introduced. When $o_{st, hp_ice, l, t} = 1$, the heat pump is enabled for operation at that temperature level, and when $o_{st, hp_ice, l, t} = 0$, the operation is disabled. Furthermore, for each temperature level l , a storage content bound $Q_{st, hp_ice, l}$ is precalculated as a parameter analogous to Equation (17).

The operational constraint for each temperature level l is given by

$$Q_{st, t+1} \leq Q_{st}^{\text{max}} - o_{st, hp_ice, l, t} \cdot Q_{st, hp_ice, l} \quad (20)$$

The COP of the ice-storage heat pump is modeled based on the ice-storage temperature level l and the heat carrier temperature level m by

$$\text{COP}_{hp_ice, l, m, t} = \frac{T_{m, t}}{T_{m, t} - T_{st, l, t}} \quad (21)$$

Therefore, the electricity demand of the ice-storage heat pump $P_{st, hp_ice, el, t}$ at time step t is modeled by

$$P_{st, hp_ice, el, t} = \sum_m \sum_l \frac{\dot{Q}_{hp_ice, l, m, t}^{\text{out}}}{\text{COP}_{hp_ice, l, m, t}}. \quad (22)$$

The Energy Efficiency Ratio (EER) is inversely related to the COP of a heat pump, and is given by the expression $\text{EER} = \frac{1}{\text{COP}} - 1$. The resulting cooling flow $\dot{Q}_{st, hp_ice, el, t}$ for each temperature level l can be expressed as

$$\dot{Q}_{hp_ice, l, t}^{\text{out}} = \sum_m \dot{Q}_{hp_ice, l, m, t} \left(\frac{\frac{1}{\text{COP}_{hp_ice, l, m, t}} - 1}{\text{COP}_{hp_ice, l, m, t}} \right) \quad (23)$$

Furthermore, the ice-storage heat pump is limited for its cooling power; therefore, for each temperature level l the heating flow is constrained by the following:

$$\frac{\sum_m \dot{Q}_{hp_ice, l, t}^{\text{out}}}{\dot{Q}_{hp_ice}^{\text{max}}} \leq o_{st, hp_ice, l, t}, \quad (24)$$

which ensures that the output flows do not exceed its maximum capacity $\dot{Q}_{st, hp_ice}^{\text{max}}$ when the heat pump is operational, that is, when $o_{st, hp_ice, l, t} = 1$.

In Figure 3, these interconnections are illustrated for two heat carrier temperature levels and two storage temperature levels.

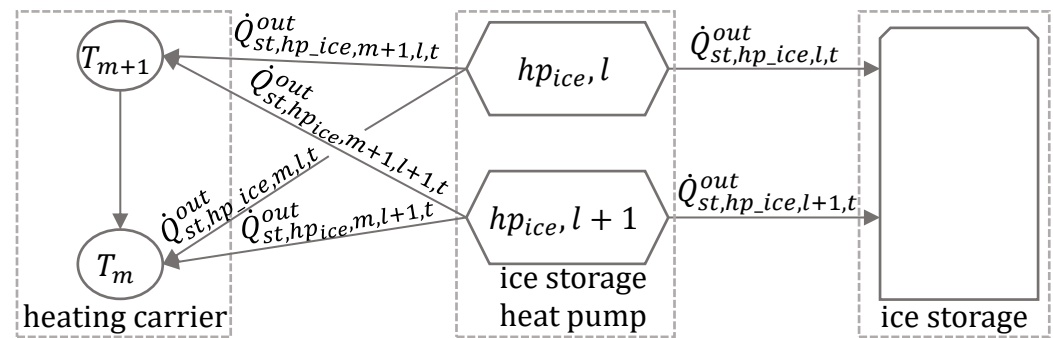


Figure 3. Flow chart of ice storage with ice-storage heat pump in and output flows for discrete temperature levels.

2.2.4. Effectiveness of Charging and Discharging

During the freezing process, the ice layer grows steadily but at an increasingly slower rate. The growing ice layer represents an increasing thermal resistance. Although the expanded surface area during freezing partially compensates for this resistance, the overall heat transfer deteriorates as the ice layer thickens. In contrast, during the melting process, the thermal resistance decreases [46].

West and Braun developed a model based on physical principles and empirical correlations to describe heat transfer performance between pipes and water or ice in ice-storage tanks. In their model, the effectiveness of heat transfer depends on the relative level of ice around the pipe, which is related to the successive layers of water and ice [51].

Dohman et al. concluded that lowering the temperature of the brine accelerates the growth of ice [52]. Castell et al. and Candanedo et al. found that the effectiveness of charging and discharging depends on the heat transfer surface area and the flow rate of the heat transfer fluid [53]. Thiem et al., based on the work of Braun et al., modeled the effectiveness as a function of the state of charge, mass flow rate, and flow temperature [31]. For medium mass flow rates, Thiem et al.'s curves align closely with those of Braun et al. Therefore, Braun et al.'s curves are used in this model for simplicity.

Furthermore, heat transfer between successive layers of water and ice, which can occur during partial charging and discharging, is not considered. This simplification helps maintain a linear model and reduces computational time, particularly for seasonal ice-storage applications.

For modeling the nonlinear behavior of the effectiveness curve, a stepwise linearization using a convex hull is applied to not introduce further binary variables. Here, the effectiveness c is the dimensionless ratio of actual to ideal heat transfer between the heat transfer fluid and the storage. The linear segments use b as the y-intercept and m as the slope; physically, b is the initial effectiveness with no ice, while m captures how effectiveness changes as the ice layer grows or shrinks. The charging curve is linearized with $s = 2$ segments, meanwhile, the discharging curve, which is nearly linear, is approximated using an $s = 1$ segment. The heat transfer effectiveness curves with their linearization are illustrated in Figure 4.

As shown in Tables A1 and A2, the piecewise-linear convex-hull approximation reproduces the original effectiveness curves with small deviations: for charging, the relative error remains within $\pm 5\%$ (average 2.1% over six evaluated X_{ice} points), and for discharging within $\pm 13\%$ (average 5.6% over six points), which is acceptable for engineering accuracy while significantly reducing computational complexity.

However, to avoid additional binary constraints, the effectiveness curves must account for both the liquid and frozen phases of the storage system. The effectiveness curves shown in Figure 4 only consider the ice phase. Therefore, a shift of the linearized curves

is necessary to include the liquid phase of the storage in relation to the storage capacity, which includes both the liquid and frozen phases. To adjust for this, we shift the charging and discharging curves horizontally to reflect the capacity contribution of the liquid phase.

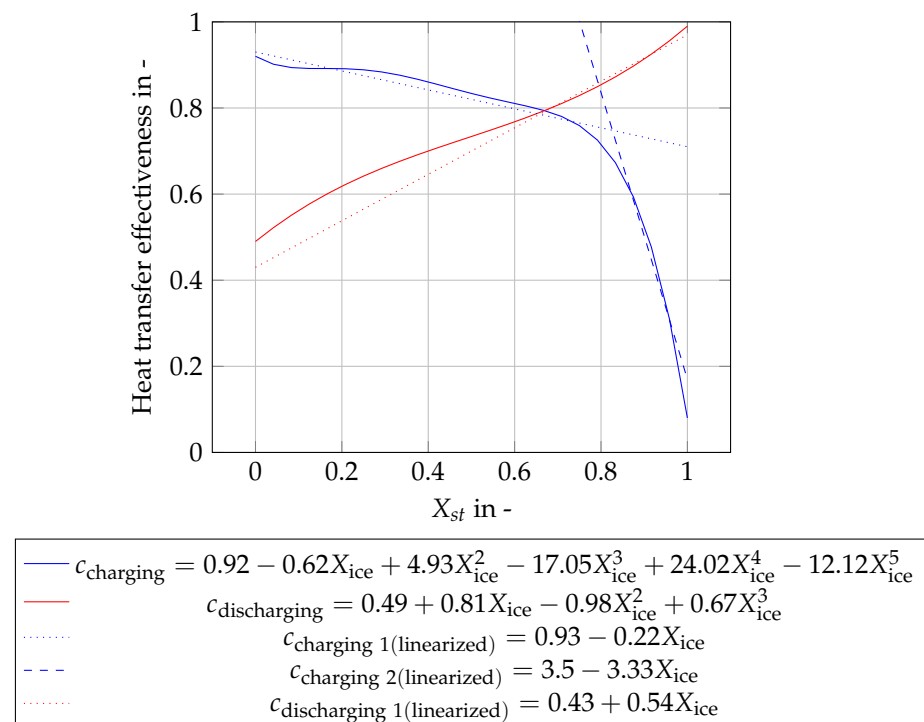


Figure 4. Heat transfer effectiveness curves with linearization for charging and discharging from Thiem et al. (Ice phase only).

The horizontal shift accounts for this difference by adjusting the linearized curves according to the ratio of the liquid phase to the total storage capacity. For charging, a new y-intercept, denoted as b^* , and a new slope, denoted as m^* are calculated. For discharging, we do not perform the shifting. While this simplification may slightly overestimate the discharging efficiency, it eliminates the need for an additional binary constraint, thus reducing model complexity. Figure 5 illustrates, for a liquid storage capacity of 20% and a frozen storage capacity of 80%, the shifted linearized curves.

λ^{in} and λ^{out} represent the resulting charging and discharging efficiencies, respectively. For the temperature level n , the maximum value of λ_n^{in} is determined by the unshifted y-intercept, $\max(b_n^{\text{in}})$, which ensures that the charging efficiency does not exceed this value since $b_n^{\text{in}} < b_n^{*\text{in}}$.

The linearized charging and discharging constraints are given by the following equations:
For the charging curve:

$$m_n^{*\text{in}} \cdot \frac{Q_{st,t+1}}{Q_{st}^{\text{max}}} + b_n^{*\text{in}} \geq \lambda_n^{\text{in}} \quad (25)$$

$$\lambda_n^{\text{in}} \geq \frac{Q_{st,t}^{\text{in}}}{Q_{st}^{\text{in,max}}}, \quad 0 \leq \lambda_n^{\text{in}} \leq \max(b_n^{\text{in}}) \quad (26)$$

For the discharging curve:

$$m_n^{\text{out}} \cdot \frac{Q_{st,n,t+1}}{Q_{st}^{\text{max}}} + b_n^{\text{out}} = \lambda_n^{\text{out}} \quad (27)$$

$$\lambda_n^{\text{out}} \geq \frac{\dot{Q}_{\text{st},n,t+1}^{\text{out}}}{\dot{Q}_{\text{st}}^{\text{out,max}}}, \quad \min(b_n^{\text{out}}) \leq \lambda_n^{\text{out}} \leq 1 \quad (28)$$

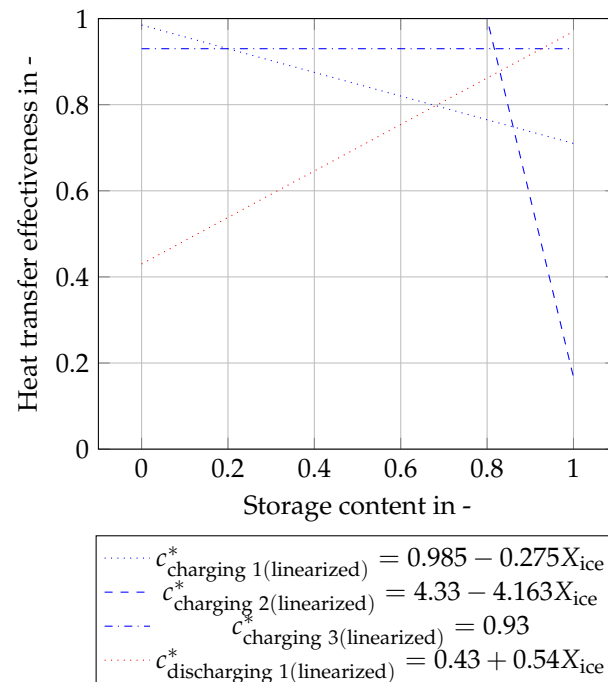


Figure 5. Heat transfer effectiveness curves with linearization for charging and discharging for the storage content including both phases.

2.2.5. Objective Function

The operational principles and constraints for components not explicitly detailed in this work, such as battery, electrical heater and heat pump, are formulated as introduced in Section 1.3 with the approaches provided by oemof [47,54] and MTRESS [48] and are explained in previous works. These references comprehensively describe the energy flow modeling, efficiency calculations, and decision variables required for such components.

The objective function of the operation is designed to minimize the total system cost (C) while ensuring the operational constraints and energy flows of the ice-storage system, and its associated components are respected. It is formulated as

$$C = \sum_t \left(c_{\text{elec,grid}} \cdot P_{\text{elec,grid},t} + c_{\text{elec,ren}} \cdot P_{\text{elec,ren},t} \right) \quad (29)$$

Here, $c_{\text{elec,grid}}$ and $c_{\text{elec,ren}}$ are the costs per unit of electricity consumed from the grid and from renewable sources, respectively, all expressed in EUR/kWh. The terms $P_{\text{elec,grid},t}$ and $P_{\text{elec,ren},t}$ denote the power consumption from the grid and renewable sources at time t .

2.3. Time-Series Aggregation Method for Three Time Layers

First, we want to give an overview of relevant time indices introduced in the work of Kotzur et al. Each original time step t is represented by a time step g , within a period i . In the case where periods are aggregated into typical periods, each original candidate period i is assigned to a group or cluster $i \in K_k$, which is represented by a typical period k . Conversely, a typical period for each candidate period can be determined using a look-up table such that $k = f(i)$.

The storage content is modeled as a superposition of the intra $Q_{\text{st},k,g}^{\text{intra}}$ and the inter storage content $Q_{\text{st},i}^{\text{inter}}$. The intra storage content models the change of the storage in a typical period, while the inter storage content describes the states at the beginning of each

period [44]. The superposition of both storage contents results in a storage content $Q_{st,t}$ (Equation (30)):

$$Q_{st,t} = Q_{s,f(i(t)),g(t)}^{\text{intra}} + Q_{st,i(t)}^{\text{inter}} \quad (30)$$

At this point, there has been no investigation into the treatment of relevant decision variables, which are either binary $x \in \{0, 1\}$ or continuous $x \in [0, 1]$. There are two possible approaches to model these variables:

A. Intra-period modeling (IPM):

The relevant binary variables ($x_{st,k,g}$) are modeled on the same time layer as the intra-period storage content, which allows the state variable to be calculated for each time step g within a typical period k .

B. Full-resolution modeling (FRM):

The relevant binary variables ($x_{st,t}$) are modeled on a separate time layer, representing each original time step t of the observation period.

The modeling with the inter-period approach is not implemented, as it would introduce excessive inaccuracies for the research questions at hand. The approach **A** represents the status quo of the TSA method, which considers two separate time layers. The approach **B** results in three distinct time layers, adding computational complexity but maintaining a high level of detail in the optimization process.

3. Case Study: Brainergy Park Jülich

Brainergy Park Jülich is an emerging 60-hectare industrial area near Jülich, North Rhine-Westphalia in Germany, managed by Brainergy Park Jülich GmbH, a joint venture of Jülich and the neighboring municipalities Niederzier and Titz. The park is divided into two sections: the “Village”, focused on office and research buildings, and the “Industrial” area for offices, manufacturing, and workshops. The Village will also include the Brainergy Hub, a center for innovation and startups, aimed at supporting the energy transition, fostering synergies between research and industry, and promoting sustainable employment.

3.1. System Description

The Brainergy Park aims to be a flagship project for the energy transition, utilizing a high share of renewable energy sources combined with an innovative and intelligent energy management system. At the core of this system is a highly integrated thermal network that connects all buildings within the park, allowing for the efficient distribution and exchange of thermal energy. This network supports the concept of buildings as “prosumers”, enabling them to function as both energy consumers and producers.

The central energy hub of the park is designed to operate the network with variable supply temperatures, ranging from 12 °C (cooling) to 18 °C (heating) throughout the year, optimizing both heating and cooling demands. The heating demand of all buildings supplied by the network is approximated to be 5090 MWh/a; meanwhile, the cooling demand is 4045 MWh/a. The energy hub is connected to a nearby PV and wind park, which allows for the use of renewable electricity at a lower cost compared to the grid cost: the economic parameters are shown in Table A4. Moreover, the hub is equipped with advanced heat pumps, which draw energy primarily from external air heat exchangers, as well as an ice-storage system with an ice-storage heat pump, which uses the storage as an exergy source. The air temperature for the air heat exchanger, as well as the ground temperature for ice-storage losses, the generation profiles of the renewable sources, and the heating and cooling load are depicted in Figure 6.

Additionally, the energy hub includes an electric boiler that ensures the operational reliability of the heat pumps, especially during low-temperature periods, while also having

the capacity to support the electricity market. A battery supports the daily decoupling of electricity demand and generation. Figure 7 provides a schematic of the energy flows in both heating and cooling modes for this system. The yellow arrows indicate the flow of electricity from the power grid and renewable sources to various components such as the battery, electrical heater, and heat pump. Grey arrows represent the thermal flow. On the heating mode side (left), the heat pump supplies the heating demand, while in cooling mode (right), the ice storage supports the cooling demand by releasing stored cooling energy. The overall design of the energy system focuses on maintaining high efficiency and flexibility, ensuring that energy supply meets demand in the most sustainable manner possible.

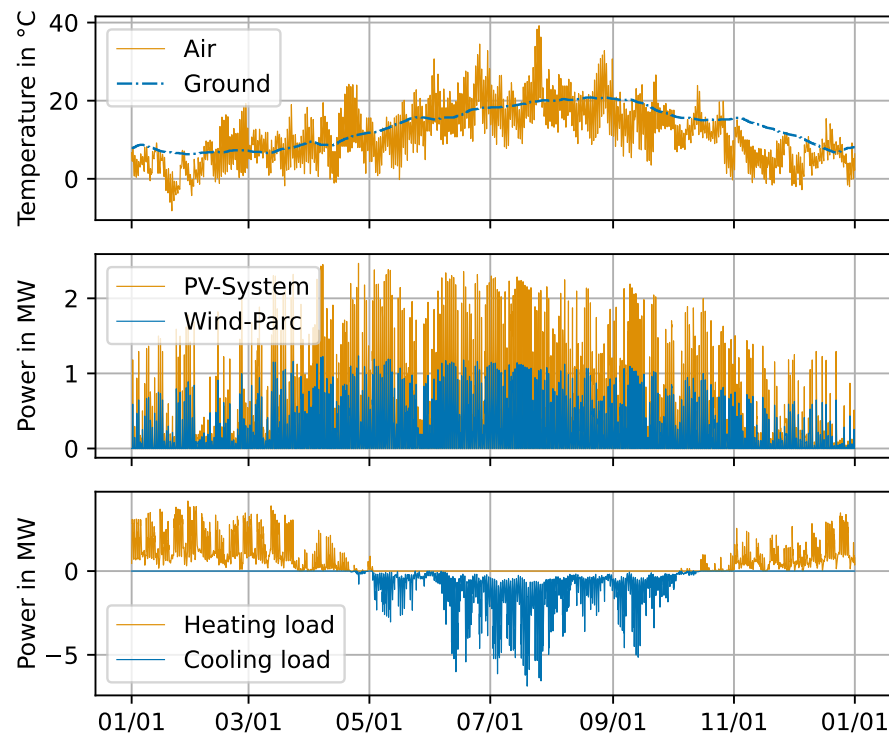


Figure 6. Annual time-series of heating and cooling demand, outdoor and ground temperatures, and usable wind and PV power at Brainergy Park.

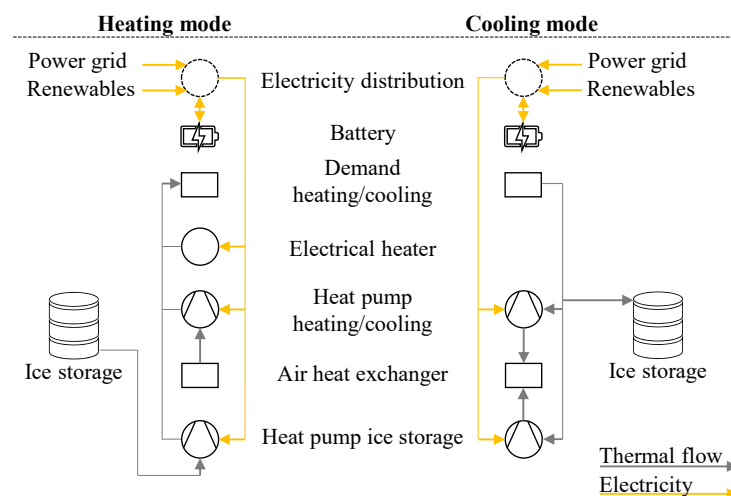


Figure 7. Schematic representation of the generation structure in the energy center at Brainergy Park Jülich, heating mode on the left and cooling mode on the right.

3.2. Parameters for the Operational Optimization Procedure

The parameterization of the energy for the operational optimization, as shown in Figure 7, procedure is outlined in Table A3. The storage level must be the same in the first and last time step of the year. Additionally, discrete temperature levels for heating, cooling, and ice-storage interactions are defined as shown in Table A5. The investigated ice-storage capacity is presented in Table 2. Additionally, analyses were conducted for other capacities; however, these did not yield new insights and are therefore not discussed further in the paper.

Table 2. Ice-storage parameters with corresponding height and volume.

| Diameter (m) | Height (m) | Volume (m ³) |
|--------------|------------|--------------------------|
| 6.196 | 5 | 150.8 |

4. Results and Discussion

This section presents an analysis of the energy system performance with and without TSA. In Section 4.1, we first analyze the energy flows of the reference system without TSA. In Section 4.2, we then introduce selected Key Performance Indicators (KPIs). Finally, in Section 4.3, we evaluate the performance and efficiency of the additional time layer for TSA introduced in Section 2.3. The k-medoids cluster method is used for TSA. Furthermore, the effectiveness of the charging and discharging processes within the model is influenced by both the storage level and the aggregate state of the storage tank. To evaluate the computational impact of TSA, both scenarios (with and without effectiveness curves) are examined. All computations are performed in Python 3.10 using Gurobi 11.0 on a Dell Precision T5810 workstation (Intel Xeon E5-1650 v3 @ 3.5 GHz, 64 GB RAM, NVIDIA Quadro K620, DELL GmbH, Frankfurt am Main, Germany).

4.1. Operation of Energy System Without Time-Series Aggregation

Figure 8 depicts the operation of the thermal energy system components without TSA, by not considering charging and discharging efficiency. In the winter, the ice-storage heat pump primarily utilizes the ice storage as a thermal source to provide heating and to freeze the ice storage further. In contrast, during the summer, the ice-storage heat pump predominantly uses ambient air to supply cooling. Despite its versatility, the ice-storage heat pump contributes only a small portion of the total energy supply compared to the primary heat pump for heating and cooling.

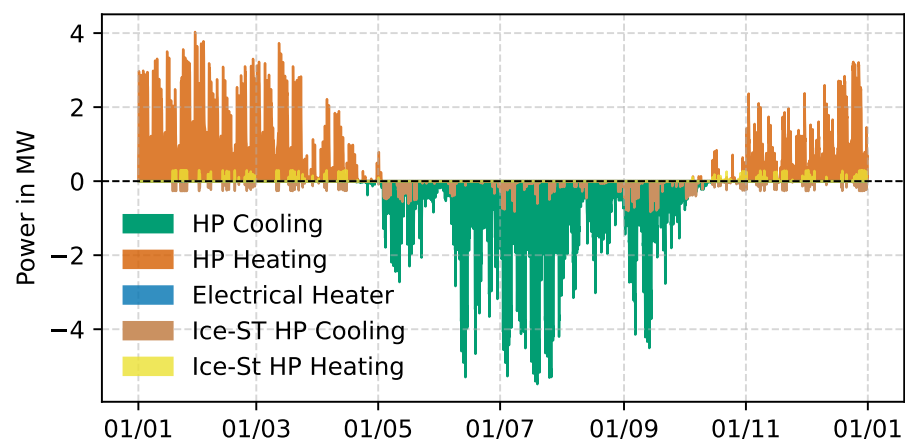


Figure 8. Annual operation of thermal energy system components for heating and cooling, without considering charging and discharging efficiency.

This operational behavior reflects the system's design to prioritize conventional heat pump operation for efficiency, while the ice-storage system provides supplementary thermal energy when needed. As described in Section 2.2.3, the ice-storage heat pump is modeled with discrete temperature levels. Figure 9 shows the cooling power output from the ice-storage heat pump for discrete ice-storage temperature levels. The 'Aggregate Change' line separates the liquid phase (above) and frozen phase (below) of the storage. It illustrates the correct relationship between discrete temperature levels and the preference for heat provision at higher ice-storage temperature levels due to a better COP.

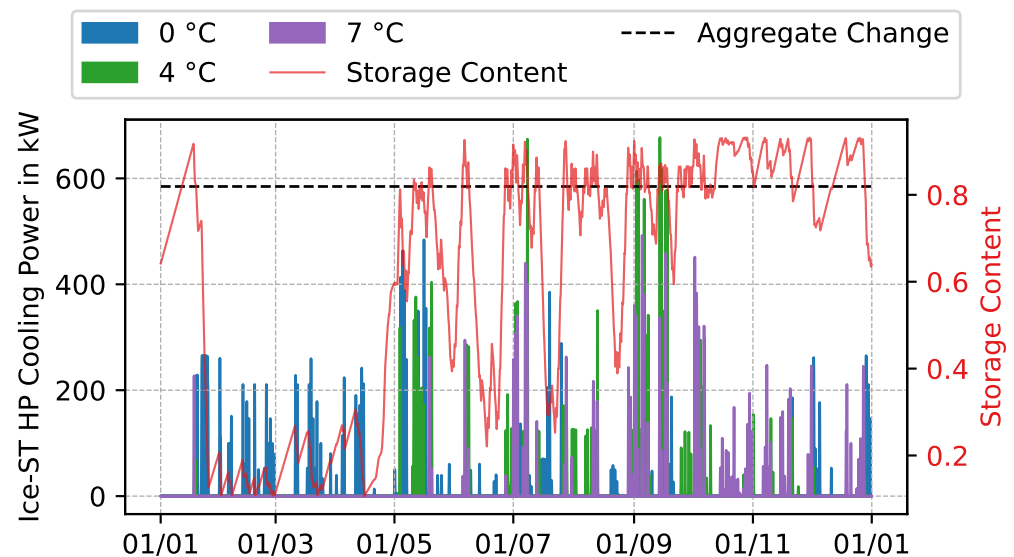


Figure 9. Annual ice-storage heat pump cooling power flows for discrete ice-storage temperatures. The 'Aggregate Change' line separates the liquid phase (above) and frozen phase (below) of the storage.

4.2. Key Performance Indicators

The KPIs are used to assess the deviation from the reference scenario when applying TSA. The scenarios involving TSA are categorized into two strategies, as defined in Eq. (30), denoted by \mathcal{S} , where $\mathcal{S} \in \{A, B\}$. For each strategy, the analysis is carried out across varying numbers of typical periods p .

4.2.1. Optimization and Performance Metrics

The first metric is the relative difference in the objective value of the optimization, expressed as

$$\text{RelDiff}_{\text{Cost}}(p, \mathcal{S}) = \frac{|C(p, \mathcal{S}) - C_{\text{ref}}|}{C_{\text{ref}}} \cdot 100. \quad (31)$$

Here, $C(p, \mathcal{S})$ represents the objective value for the aggregated model with p typical periods and strategy \mathcal{S} , while C_{ref} corresponds to the objective value for the reference scenario without TSA.

The second metric is the computational time required to compute the optimization results.

4.2.2. Technical Performance Indicators

The Seasonal Energy Efficiency Ratio (SEER) represents the annual efficiency of the ice-storage heat pump. Its relative difference from the reference case is given by

$$\text{RelDiff}_{\text{SEER}}(p, \mathcal{S}) = \frac{|\text{SEER}(p, \mathcal{S}) - \text{SEER}_{\text{ref}}|}{\text{SEER}_{\text{ref}}} \cdot 100, \quad (32)$$

where

$$\text{SEER}(p, \mathcal{S}) = \frac{\sum_t \dot{Q}_{hp_ice,t}^{\text{out}}(p, \mathcal{S})}{\sum_t P_{hp_ice,t}(p, \mathcal{S})},$$

$$\text{SEER}_{\text{ref}} = \frac{\sum_t \dot{Q}_{hp_ice,t,\text{ref}}^{\text{out}}}{\sum_t P_{hp_ice,t,\text{ref}}}.$$

Additionally, the standard deviation of the storage content difference between the aggregated model and the reference case is calculated hourly as

$$\text{Storage Content Standard Deviation} = \sum_t \text{std}(Q_{st,t}(p, \mathcal{S}) - Q_{st,t,\text{ref}}). \quad (33)$$

4.3. Comparison of Ice-Storage Operation with and Without Time-Series Aggregation

When considering the effectiveness of charging and discharging, Figure 10 depicts the storage content for the intra-period modeling method (IPM) over the course of a year, compared to the reference storage content without TSA. Similarly, Figure 11 illustrates the storage content for the full-resolution modeling method (FRM).

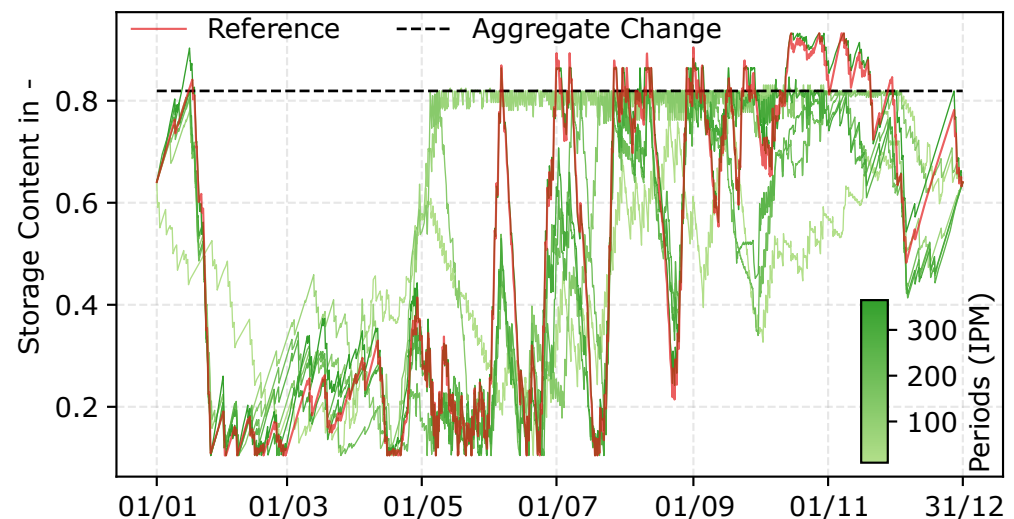


Figure 10. Annual storage content for the number of typical periods with Intra-period modeling (IPM), with considering charging and discharging efficiency. The 'Aggregate Change' line separates the liquid phase (above) and frozen phase (below) of the storage.

For both methods, the storage content across typical periods generally aligns with the reference storage content. However, distinct patterns emerge: in the FRM method, the storage content frequently exceeds the aggregate change threshold, indicating transitions into the liquid phase of the storage for fewer typical periods. Conversely, in the IPM method, the storage content closely follows the aggregate change but remains confined to the partially frozen phase. These observations highlight the differences in precision and

representation between the two modeling approaches, which are further analyzed based on optimization and performance metrics as well as technical performance indicators.

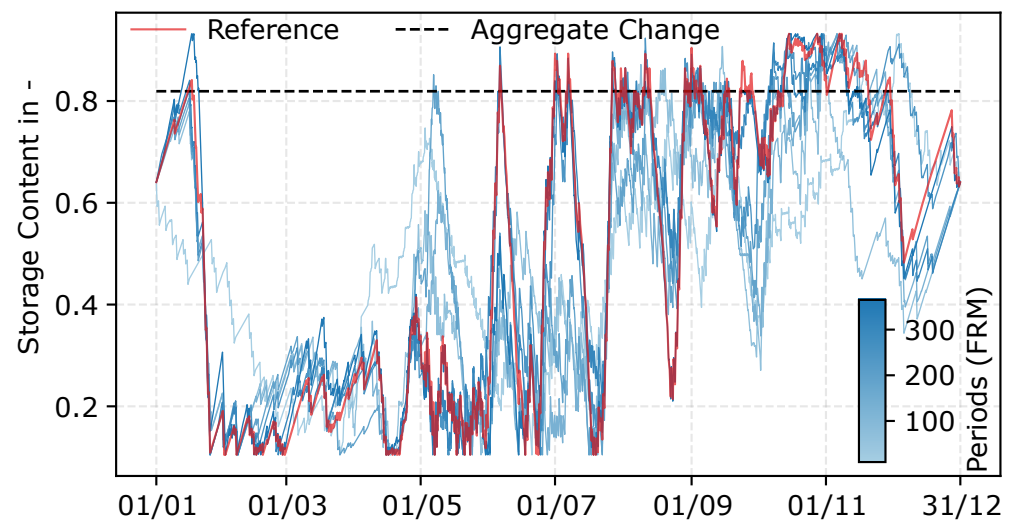


Figure 11. Annual storage content for the number of typical periods with full-resolution modeling (FRM), with considering charging and discharging efficiency. The 'Aggregate Change' line separates the liquid phase (above) and frozen phase (below) of the storage.

For cases without the consideration of charging and discharging effectiveness, the storage content for the IPM method is shown in Figure A1, and for the FRM method in Figure A2.

A quantitative comparison of both modeling approaches is provided in the subsequent Sections 4.3.1 and 4.3.2, where optimization and performance metrics as well as technical performance indicators are analyzed. The key numerical results are summarized in Table A6, which highlights representative values rather than the complete data set.

4.3.1. Analysis of Optimization and Performance Metrics

Figure 12, which excludes the consideration of charging and discharging efficiency, and Figure 13, which incorporates this consideration, illustrate the deviation of the objective value and computational time as a function of the number of typical periods for intra-period modeling (IPM) and full-resolution modeling (FRM).

In both figures, the deviation of the objective value (blue lines) is nearly identical for both IPM and FRM across all numbers of typical periods. As the number of typical periods increases, the deviation in the objective value consistently decreases, demonstrating improved accuracy with higher temporal resolution.

The deviation in computational time (orange lines) shows significant variability, particularly for IPM. Computational time generally increases with the number of typical periods, reflecting the higher computational demands associated with modeling more detailed time-series. In the case without consideration of charging and discharging (Figure 12), an almost constant increase in computational time is observed, typically remaining below the reference time; at $p = 110$ typical periods, the objective-value deviation is $\leq 2.5\%$ for both IPM and FRM, and the computational time is reduced by $\sim 80\%$ (IPM) and $\sim 40\%$ (FRM) relative to the full-resolution reference.

However, when charging and discharging are considered (Figure 13), the computational time for IPM becomes highly discontinuous and exceeds the reference time starting from $p = 110$. In contrast, for FRM, the increase in computational time is more grad-

ual but remains above the reference time from around $p = 140$. From $p = 110$ on, the objective-value deviation is $\leq 2.5\%$ for both IPM and FRM.

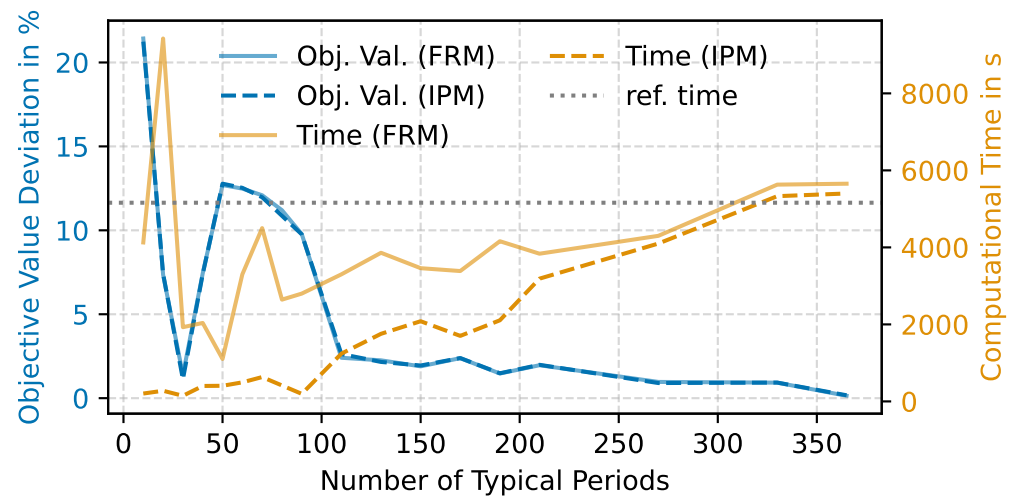


Figure 12. Deviation of objective value and computational time as a function of the number of typical periods, without considering charging and discharging efficiency.

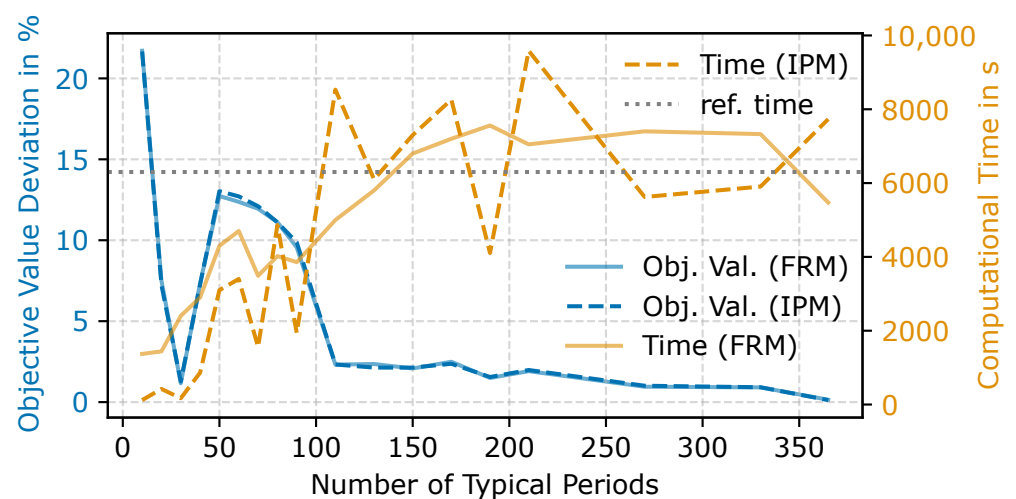


Figure 13. Deviation of objective value and computational time as a function of the number of typical periods, with considering charging and discharging efficiency.

These results highlight that, while the deviation in the objective value improves consistently for both methods with more typical periods, the behavior of computational time differs substantially between IPM and FRM.

4.3.2. Analysis of Technical Performance Indicators

Figures 14 and 15 show the deviation of the SEER from the reference scenario for IPM and FRM, with and without considering charging and discharging efficiency, respectively.

In both figures, the SEER for FRM is consistently equal to or higher than that for IPM across the range of typical periods. This can be attributed to the enhanced ability of FRM to model transitions into the liquid phase of the ice storage, thereby improving heat-pump efficiency (see Section 2.2.3). The deviation in SEER for both strategies decreases as the number of typical periods increases.

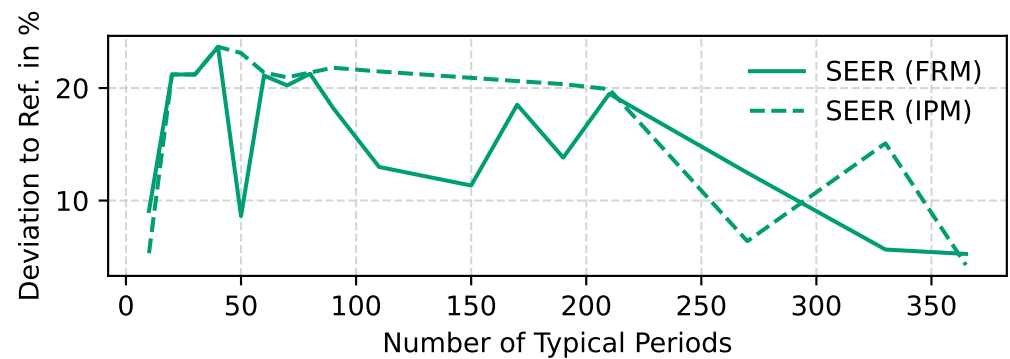


Figure 14. Deviation of the SEER as a function of the number of typical periods, without considering charging and discharging efficiency.

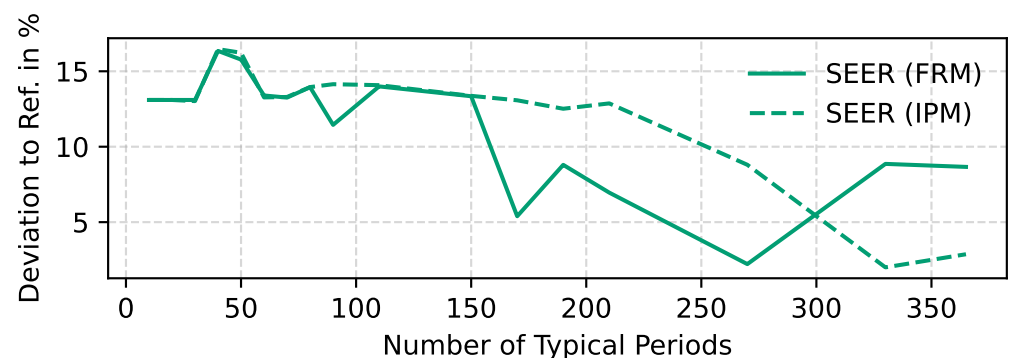


Figure 15. Deviation of the SEER as a function of the number of typical periods, with consideration of charging and discharging efficiency.

In the case without consideration of charging and discharging (Figure 14), a noticeable improvement in SEER accuracy is observed for FRM starting from $p = 90$ typical periods; at $p = 110$, the deviation is roughly 9% smaller compared to IPM. When charging and discharging are considered (Figure 15), FRM again outperforms IPM, with improvements in SEER deviation becoming evident from about $p = 160$ typical periods onward.

These results highlight the advantage of FRM in accurately representing the liquid phase of the storage, which plays a critical role in enhancing the efficiency of the ice-storage heat pump. In contrast, the IPM method shows slightly lower SEER values due to its more limited ability to model transitions into the unfrozen state.

Figures 16 and 17 depict the standard deviation of the hourly storage content as a function of the number of typical periods for IPM and FRM, with and without considering charging and discharging efficiency, respectively.

In Figure 16, where charging and discharging efficiency are not considered, the standard deviation decreases as the number of typical periods increases. This indicates improved alignment with the reference storage content at higher temporal resolutions. Both methods, IPM and FRM, show similar behavior, though no consistently superior performance between them is evident.

In contrast, Figure 17, which incorporates charging and discharging efficiency, highlights a more pronounced difference. Here, the standard deviation for FRM remains consistently lower than for IPM across most typical periods, reflecting the improved precision in representing the hourly storage content in FRM. This observation underscores the benefit of full-resolution modeling when charging and discharging efficiency are considered, as it better captures the additional binary variables that arise for these efficiencies, which are more accurately represented in FRM.

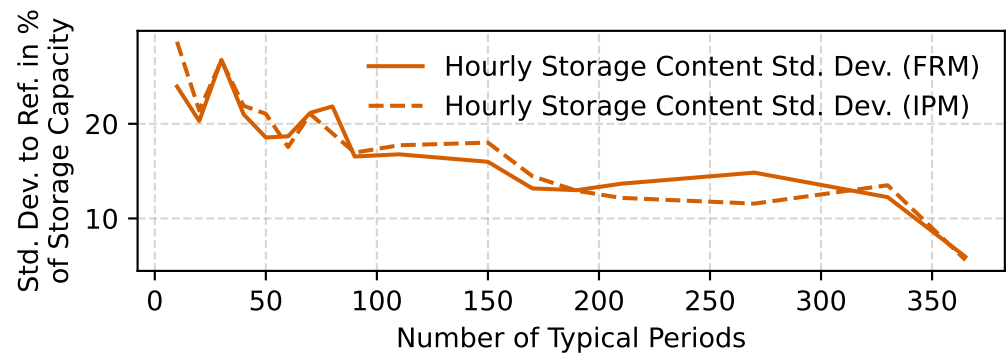


Figure 16. Standard deviation of the hourly storage content as a function of the number of typical periods, without considering charging and discharging efficiency.

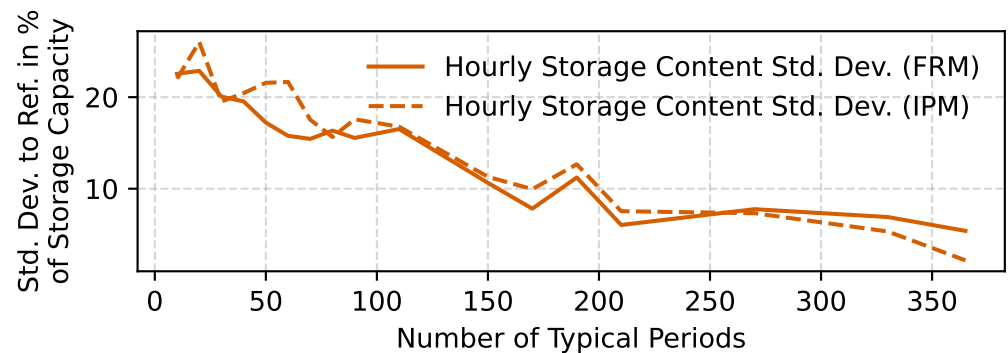


Figure 17. Standard deviation of the hourly storage content as a function of the number of typical periods, with consideration of charging and discharging efficiency.

5. Discussion

The results indicate that TSA can substantially reduce computational effort while maintaining a small deviation in the objective value relative to the full-resolution reference. Increasing the number of typical periods monotonically improves accuracy, but runtime rises accordingly. The introduced third time layer—which augments inter- and intra-period states with selected binary state variables for phase representation—captures temperature- and phase-dependent operation more faithfully at the cost of higher computational burden. Hence, there is a clear runtime–accuracy trade-off that must be tuned to the application.

When charge/discharge effectiveness is *not* modeled, TSA delivers stable runtime reductions: at $p = 110$ typical periods, the objective-value deviation is $\leq 2.5\%$ for IPM and FRM, with runtime cuts of about 80% (IPM) and 40% (FRM) and a reduced deviation of the SEER about 22% (IPM) and 13% (FRM) versus the reference. With effectiveness active, IPM runtimes become discontinuous and exceed the reference starting from $p = 110$; FRM increases more smoothly but stays above the reference from $p = 110$, while deviations remain $\leq 2.5\%$ from $p = 110$ onward.

A consistent pattern emerges when contrasting IPM and FRM. FRM more accurately represents transitions into the liquid phase of the storage and, when charging/discharging effectiveness is considered, yields systematically higher seasonal performance (e.g., SEER) and lower hourly storage-content deviations. IPM, while often faster at low to moderate numbers of typical periods, shows a stronger sensitivity of solve time once effectiveness curves and additional binaries are active. The method choice should therefore reflect the required fidelity of phase transitions and temperature coupling versus available computation time.

Modeling charging and discharging effectiveness materially affects both dispatch and computational characteristics. The convex-hull linearization used here reproduces the dominant trends without introducing further binaries, but its accuracy depends on the segmentation and on the share of sensible versus latent capacity. Moreover, the discrete temperature-level formulation is central; it links storage and system temperatures to component performance (heat-pump COP) and, thus, to both cost and feasibility, but it increases the dimensionality of the problem.

Moreover, the results indicate that the ice-storage subsystem is not the dominant cost driver within the overall energy system as reflected by the small and nearly identical objective-value deviations for both IPM and FRM observed for typical periods above $p = 110$. For instance, at $p = 110$, when charging and discharging effectiveness are not considered, FRM exhibits an approximately 9% lower SEER deviation and a 2% lower storage-content standard deviation compared to IPM, indicating that a more optimal ice-storage operation can be attained without significant economic benefits.

These findings, however, remain conditioned on several simplifying assumptions (e.g., perfect mixing, linearized effectiveness segments, and fixed temperature levels), which may bias absolute performance metrics but are not expected to affect the relative comparison between TSA configurations or modeling approaches (IPM vs. FRM). These simplifications retain the dominant physics at tractable computational cost and, relative to existing seasonal operation models, increase fidelity: perfect mixing sidesteps weakly identifiable stratification with minimal impact on seasonal KPIs; convex-hull linearization captures key nonlinearities without extra binaries; and discrete temperature levels preserve COP coupling.

While the case study reflects the specific climate and infrastructure of Brainergy Park Jülich, the framework is broadly applicable. Adapting it to other climates or building types mainly requires adjusting temperature, load, and technology parameters. Its techno-economic benefits are particularly pronounced in regions with cooling needs in summer and heating demand in winter, where variable-temperature operation and storage utilization enhance overall efficiency and cost effectiveness.

6. Conclusions

This paper proposes a MILP-based framework for the seasonal operational optimization of ice storage that couples phase-state representation (latent and sensible parts), discrete temperature levels, and linearized charge/discharge effectiveness with TSA to reduce computational time. Specifically, we extend the standard two-layer inter-/intra-period formulation by adding a third time layer for selected binary variables, preserving phase change, temperature- and COP-dependent behavior under aggregation. The approach maintains high physical fidelity while enabling tractable solve times.

Key findings are as follows:

- (i) TSA substantially reduces computational effort while maintaining high accuracy, particularly when charging and discharging effectiveness is not modeled, indicating stable performance under reduced binary complexity;
- (ii) Once effectiveness curves are introduced, runtime stability decreases due to the additional binary constraints, emphasizing a trade-off between model realism and computational efficiency;
- (iii) Compared to IPM, FRM better captures liquid-phase operation and associated efficiency effects when effectiveness curves are active;
- (iv) The added third time layer enhances the representation of temperature- and phase-dependent behavior but introduces a runtime–accuracy balance that must be tuned to the application.

Application to Brainergy Park Jülich demonstrates real-world feasibility. The integrated heat–cooling management with on-site renewables shows how seasonal ice storage can enhance energy efficiency and reduce grid reliance, while providing operational flexibility for both heating and cooling throughout the year.

Practically, the framework supports planners in selecting TSA resolution and modeling detail commensurate with decision needs and available compute. At the same time, embedding binary variables within TSA raises model complexity. Future work should quantify this impact on computational performance, refine multi-layer TSA operational optimization, explore mitigation strategies such as the selective relaxation or aggregation of binary decisions, and relax simplifying assumptions (fully mixed tank, fixed temperature levels, and linearization) to narrow the gap to detailed physics where such fidelity is critical. Furthermore, this study relies on simulation verification, and future research should focus on comparing these simulation results with measured data to validate the method’s accuracy in real-world applications.

Author Contributions: Conceptualization, M.H. and P.S.; methodology, M.H.; software, M.H.; validation, M.H., P.S. and P.G.; formal analysis, M.H., P.S. and P.G.; investigation, M.H.; data curation, M.H. and P.G.; writing—original draft preparation, M.H.; writing—review and editing, M.H., P.S. and P.G.; visualization, M.H.; supervision, B.H.; project administration, B.H.; funding acquisition, B.H. All authors have read and agreed to the published version of the manuscript.

Funding: This research received no external funding.

Data Availability Statement: Data available on request due to legal restrictions.

Acknowledgments: Supported by the Brainergy Park Jülich (BPJ) with a commissioned ice-storage engineering firm, concept papers and feasibility studies. During the preparation of this study, the authors used ChatGPT (version 4) for the purposes of text correction and improvement. The authors have reviewed and edited the output and take full responsibility for the content of this publication.

Conflicts of Interest: The authors declare no conflicts of interest.

Abbreviations

The following abbreviations are used in this manuscript:

| | |
|--------|--|
| COP | Coefficient of Performance |
| DP | Dynamic Programming |
| EER | Energy Efficiency Ratio |
| EA | Evolutionary Algorithm |
| FRM | Full-resolution modeling |
| IPM | Intra-period modeling |
| KPI | Key Performance Indicator |
| MILP | Mixed-Integer Linear Programming |
| MINLP | Mixed-Integer Nonlinear Programming |
| MIQP | Mixed-Integer Quadratic Programming |
| MPC | Model Predictive Control |
| MTRESS | Model Template for Residential Energy Supply Systems |
| oemof | open energy modeling framework |
| PCM | Phase Change Materials |
| SEER | Seasonal Energy Efficiency Ratio |
| TES | Thermal Energy Storage |
| TSA | Time-series Aggregation |

Nomenclature

| | |
|---------------------------|---|
| $A_{st,surface}$ | Surface area of the ice-storage tank in m^2 |
| b_n^{in} | Y-intercept of the linear segment for the charging curve at temperature level n |
| b_n^{*in} | Horizontal shifted Y-intercept of the linear segment for the charging curve at temperature level n |
| b_n^{out} | Y-intercept of the linear segment for the discharging curve at temperature level n |
| C | Total costs of the operation in EUR |
| $c_{elec,grid}$ | Costs per unit of electricity consumed from the grid in EUR/kWh |
| $c_{elec,ren}$ | Costs per unit of electricity consumed from renewable sources in EUR/kWh |
| $c_{p,water}$ | Specific heat capacity of water in kJ/kg |
| d_{st} | Diameter of the storage tank in m |
| E | Energy in kJ |
| g | Time step in a period |
| h_f | Melting enthalpy of ice in kJ/kg |
| h_{st} | Height of the storage tank in m |
| i | Original candidate period |
| $i_{st,n,t}$ | Binary variable indicating if charging is possible at temperature level n at time t |
| k | Typical period |
| m | Discrete temperature levels for heating |
| m_n^{in} | Slope of the linear segment for the charging curve at temperature level n |
| m_n^{*in} | Horizontal shifted slope of the linear segment for the charging curve at temperature level n |
| m_n^{out} | Slope of the linear segment for the discharging curve at temperature level n |
| M | Big-M constant for binary variable constraints |
| n | Discrete temperature levels for cooling |
| $o_{st,n,t}$ | Binary variable indicating if discharging is possible at temperature level n at time t |
| $o_{st,hp_ice,l,t}$ | Binary variable indicating if the ice-storage heat pump hp_ice is operational at temperature level l at time t |
| P_t | Electricity demand in kJ at time t |
| p | Number of typical period |
| Q_{st} | Storage content in kJ |
| $Q_{st,loss}$ | Thermal loss of the storage in kJ |
| $Q_{st,t}$ | Storage content at time t in kJ |
| $Q_{st,n}$ | Storage content at discrete temperature level n in kJ |
| $Q_{st,i}^{inter}$ | Inter-period storage content (state at the beginning of period i) in kJ |
| $Q_{st,k,g}^{intra}$ | Intra-period storage content for intra-period time index k and segment g in kJ |
| Q_{st}^{max} | Maximum storage capacity in kJ |
| $Q_{st,frz}^{max}$ | Maximum storage capacity for fully frozen in kJ |
| $Q_{st,liq}^{max}$ | Maximum storage capacity for liquid in kJ |
| $Q_{st,hp_ice,l}^{max}$ | Storage-content bound for the heat pump at temperature level l in kJ |
| $\dot{Q}_{m,t}^{in}$ | Heat flow as input at the temperature level m at time t in kJ/h |
| $\dot{Q}_{m,t}^{out}$ | Heat flow as output at the temperature level m at time t in kJ/h |
| $\dot{Q}_{n,t}^{in}$ | Cooling flow as input at the temperature level n at time t in kJ/h |
| $\dot{Q}_{n,t}^{out}$ | Cooling flow as output at the temperature level n at time t in kJ/h |
| $\dot{Q}_{st}^{in,max}$ | Maximum Input flow of energy into the storage at time t in kJ/h |
| $\dot{Q}_{st}^{out,max}$ | Maximum output flow of energy from the storage at time t in kJ/h |
| $\dot{Q}_{st,t}^{in}$ | Input flow of energy into the storage at time t in kJ/h |
| $\dot{Q}_{st,t}^{out}$ | Output flow of energy from the storage at time t in kJ/h |
| $\dot{Q}_{st,n,t}^{in}$ | Charging power at temperature level n at time t in kJ/h |
| $\dot{Q}_{st,n,t}^{out}$ | Discharging power at temperature level n at time t in kJ/h |
| $\dot{Q}_{hp_ice}^{max}$ | Maximum output flow of the heat pump connected to ice storage in kJ/h |

| | |
|----------------------------|--|
| $r_{m,m+1}$ | Energy reduction factor for heating transfer between temperature levels |
| $r_{n,n+1}$ | Energy reduction factor for cooling transfer between temperature levels |
| $s_{st,t}$ | Binary variable indicating storage phase (1: melting, 0: liquid) at time t |
| T_m | Discrete temperature level for heating in °C |
| T_n | Discrete temperature level for cooling in °C |
| T_{grd} | External temperature of the ground in °C |
| T_{melt} | Melting temperature of ice in °C |
| T_{st} | Storage temperature in °C |
| T_{st}^{max} | Maximum storage temperature in °C |
| t | Original time step in the full time-series |
| U_{st} | Heat transfer coefficient in $\text{W}/(\text{m}^2\text{K})$ |
| V_{st} | Volume of the storage tank in m^3 |
| X^{max} | Maximum ice level |
| X_{st} | Ice level in the storage tank (range 0 to 1) |
| $x_{st,k,g}$ | Binary or continuous decision variable indexed for intra-period modeling (IPM), at time step g within typical period k |
| $x_{st,t}$ | Binary or continuous decision variable indexed for full-resolution modeling (FRM), at time step t |
| $\delta_{st,t}$ | Self-discharge loss rate of the storage at time t |
| $\eta_{st,t}^{\text{in}}$ | Charging efficiency of the storage at time t |
| $\eta_{st,t}^{\text{out}}$ | Discharging efficiency of the storage at time t |
| λ | Thermal conductivity in $\text{W}/(\text{mK})$ |
| λ^{in} | Charging efficiency of the ice storage |
| λ^{out} | Discharging efficiency of the ice storage |
| ρ_{ice} | Density of ice in kg/m^3 |
| ρ_{water} | Density of water in kg/m^3 |

Appendix A

Table A1. Charging effectiveness: original vs. piecewise-linear.

| $X_{\text{ice in}}$ | c_{orig} | c_{lin} | Abs. Error | Rel. Error in % |
|---------------------|-------------------|------------------|------------|-----------------|
| 0.15 | 0.897 | 0.897 | 0.000 | 0.006 |
| 0.30 | 0.872 | 0.864 | −0.008 | −0.986 |
| 0.45 | 0.834 | 0.831 | −0.003 | −0.354 |
| 0.60 | 0.808 | 0.798 | −0.010 | −1.305 |
| 0.75 | 0.731 | 0.765 | 0.034 | 4.597 |
| 0.90 | 0.531 | 0.503 | −0.028 | −5.329 |

Table A2. Discharging effectiveness: original vs. linear.

| $X_{\text{ice in}}$ | c_{orig} | c_{lin} | Abs. Error | Rel. Error in % |
|---------------------|-------------------|------------------|------------|-----------------|
| 0.15 | 0.592 | 0.511 | −0.081 | −13.640 |
| 0.30 | 0.663 | 0.592 | −0.071 | −10.694 |
| 0.45 | 0.717 | 0.673 | −0.044 | −6.150 |
| 0.60 | 0.768 | 0.754 | −0.014 | −1.813 |
| 0.75 | 0.829 | 0.835 | 0.006 | 0.735 |
| 0.90 | 0.914 | 0.916 | 0.002 | 0.259 |

Table A3. Technological components and key parameters, specified in consultation with a commissioned ice-storage engineering firm and consistent with BPJ concept papers and feasibility studies.

| Component | Parameter | Value | Unit |
|----------------------------|-------------------------------|-------------|-----------------------|
| Air Heat Exchanger | Air Temperature | time series | °C |
| Battery Storage | Nominal Capacity | 1000 | kWh |
| | Charging Efficiency | 98 | % |
| | Discharging Efficiency | 98 | % |
| | Charging/Discharging C-Rate | 20 | % |
| Heat Pump (Cooling) | Thermal Power Limit | 5500 | kW |
| | EER for Set Temp Interval | 4.8 | - |
| | Lorenz EER In Temp | 30 | °C |
| | Lorenz EER Out Temp | 10 | °C |
| Heat Pump (Heating) | Thermal Power Limit | 4500 | kW |
| | COP for Set Temp Interval | 4 | - |
| | Lorenz COP In Temp | 10 | °C |
| | Lorenz COP Out Temp | 45 | °C |
| Heat Pump with Ice Storage | Thermal Power Limit | 1000 | kW |
| | COP for Set Temp Interval | 4 | - |
| | EER for Set Temp Interval | 4.8 | - |
| | Lorenz COP In Temp | 2 | °C |
| | Lorenz COP Out Temp | 10 | °C |
| Ice Storage | Max Storage Temp. | 10 | °C |
| | Storage Height | 6.5 | m |
| | Diameter | variable | m |
| | Initial Ice Level | 20 | % |
| | Max Ice Level | 80 | % |
| | Inflow Efficiency | 98 | % |
| | Outflow Efficiency | 98 | % |
| | Max Charging/Discharging Rate | 1 | % of storage capacity |
| Electrical Heater | Thermal Power Limit | 1000 | kW |
| Heat Demand | Flow Temperature | 18 | °C |
| | Return Temperature | 14 | °C |
| Cooling Demand | Flow Temperature | 12 | °C |
| | Return Temperature | 16 | °C |

Table A4. Economic parameters for energy sources and grid connection, specified in consultation with BPJ.

| Component | Parameter | Value | Unit |
|------------------|--------------|-------|---------|
| PV Source | Working Rate | 0.10 | EUR/kWh |
| Wind Source | Working Rate | 0.10 | EUR/kWh |
| Electricity Grid | Working Rate | 0.40 | EUR/kWh |

Table A5. Discrete temperature levels for heating, cooling, and ice-storage interactions, consistent with BPJ concept papers and feasibility studies.

| System Component | Parameter | Levels | Unit |
|-----------------------|---|----------------|------|
| Ice Storage | Ice Storage Loss Temperature Level | [3] | °C |
| Ice Storage Heat Pump | Ice Storage Source Temperature Levels (l) | [0, 4, 7] | °C |
| Heating Circuit | Flow Temperature Levels (m) | [14, 18, 30] | °C |
| Cooling Circuit | Flow Temperature Levels (n) | [0, 4, 12, 16] | °C |

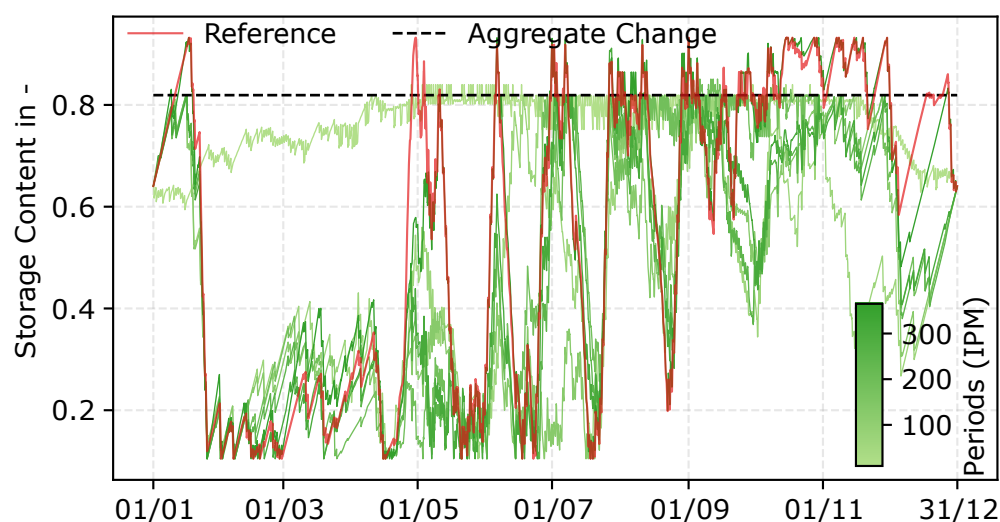


Figure A1. Annual storage content for the number of typical periods with intra-period modeling (IPM), without considering charging and discharging efficiency.

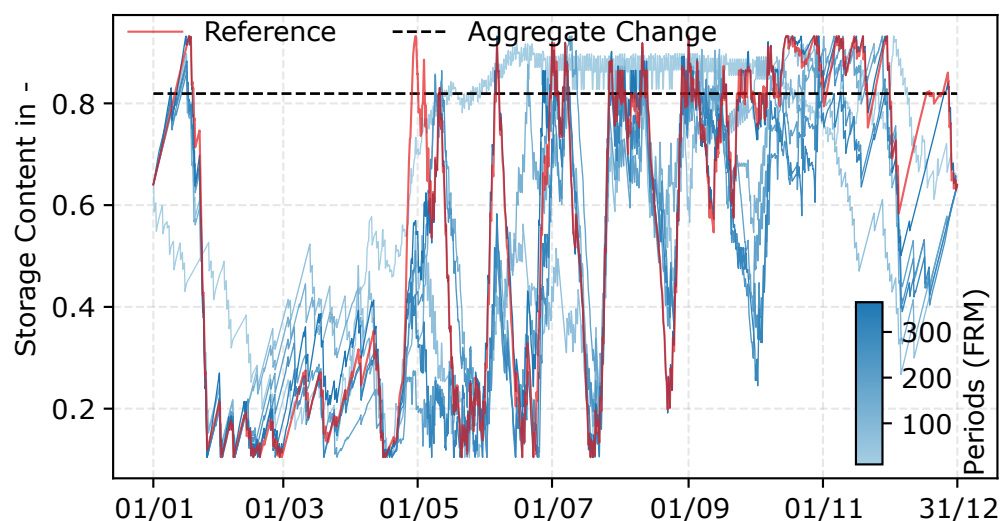


Figure A2. Annual storage content for the number of typical periods with full-resolution modeling (FRM), without considering charging and discharging efficiency.

Table A6. Comparison of performance metrics and technical performance indicators FRM vs. IPM with and without charging/discharging effectiveness.

| Performance Metrics and Technical Performance Indicators | Number of Typical Periods | Effectiveness Considered | | Effectiveness Not Considered | |
|--|---------------------------|--------------------------|-------|------------------------------|-------|
| | | FRM | IPM | FRM | IPM |
| SEER Deviation to Ref. in % | 50 | 15.50 | 16.00 | 8.54 | 23.27 |
| | 110 | 13.75 | 13.90 | 12.91 | 21.63 |
| | 170 | 10.25 | 13.12 | 18.54 | 20.54 |
| | 240 | 4.38 | 10.50 | 15.63 | 13.09 |
| | 300 | 10.31 | 10.31 | 8.90 | 19.54 |
| Std. Dev. to Ref. in % of Storage Capacity | 50 | 17.39 | 21.30 | 18.51 | 21.06 |
| | 110 | 16.30 | 16.50 | 16.38 | 17.65 |
| | 170 | 7.82 | 10.01 | 12.77 | 14.26 |
| | 240 | 6.74 | 7.60 | 14.04 | 11.91 |
| | 300 | 7.40 | 6.50 | 13.19 | 12.55 |
| Objective Value Deviation in % | 50 | 12.60 | 13.00 | 12.56 | 12.68 |
| | 110 | 2.00 | 2.01 | 2.20 | 2.68 |
| | 170 | 2.56 | 2.48 | 2.07 | 2.07 |
| | 240 | 1.63 | 1.66 | 1.47 | 1.47 |
| | 300 | 0.94 | 0.99 | 0.84 | 0.83 |
| Computational Time in s | 50 | 4453 | 3152 | 1171 | 487 |
| | 110 | 5092 | 8480 | 3283 | 1268 |
| | 170 | 7093 | 9440 | 3429 | 1707 |
| | 240 | 7146 | 7733 | 4096 | 3722 |
| | 300 | 7466 | 5813 | 5024 | 4780 |

References

- Altuntas, M.; Erdemir, D. An investigation on potential use of ice thermal energy storage system as energy source for heat pumps. *J. Energy Storage* **2022**, *55*, 105588. <https://doi.org/10.1016/j.est.2022.105588>.
- Arteconi, A.; Hewitt, N.; Polonara, F. State of the art of thermal storage for demand-side management. *Appl. Energy* **2012**, *93*, 371–389. <https://doi.org/10.1016/j.apenergy.2011.12.045>.
- Cabeza, L.F.; Martorell, I.; Miró, L.; Fernández, A.I.; Barreneche, C. (Eds.) *Introduction to Thermal Energy Storage (TES) Systems*; Elsevier: Amsterdam, The Netherlands, , 2015. <https://doi.org/10.1533/9781782420965.1>.
- Sarbu, I.; Sebarchievici, C. A Comprehensive Review of Thermal Energy Storage. *Sustainability* **2018**, *10*, 191. <https://doi.org/10.3390/su10010191>.
- Xu, J.; Wang, R.Z.; Li, Y. A review of available technologies for seasonal thermal energy storage. *Solar Energy* **2014**, *103*, 610–638. <https://doi.org/10.1016/j.solener.2013.06.006>.
- Dahash, A.; Ochs, F.; Janetti, M.B.; Streicher, W. Advances in seasonal thermal energy storage for solar district heating applications: A critical review on large-scale hot-water tank and pit thermal energy storage systems. *Appl. Energy* **2019**, *239*, 296–315. <https://doi.org/10.1016/j.apenergy.2019.01.189>.
- Desai, F.; Prasad, J.S.; Muthukumar, P.; Rahman, M.M. Thermochemical energy storage system for cooling and process heating applications: A review. *Energy Convers. Manag.* **2021**, *229*, 113617. <https://doi.org/10.1016/j.enconman.2020.113617>.
- Xia, T.; Ji, J.; Ke, W. Case study of variable speed photovoltaic direct-driven ice-storage air conditioning system in Wuhu. *Appl. Therm. Eng.* **2024**, *248 Pt A*, 122896. <https://doi.org/10.1016/j.applthermaleng.2024.122896>.
- Qiang, W.; Liao, Y.; Deng, J.; Peng, C.; Long, H.; Yang, H.; Bai, J.; Su, Y.; Wei, Q.; Xu, X.; et al. Research on systematic analysis and optimization method for ice storage cooling system based on model predictive control: A case study. *Energy Build.* **2025**, *326*, 115065. <https://doi.org/10.1016/j.enbuild.2024.115065>.
- Yang, K.S.; Chao, Y.S.; Hsieh, C.H.; Chai, M.L.; Wang, C.C. Performance of Commercially Open Refrigerated Showcases with and without Ice Storage—A Case Study. *Processes* **2021**, *9*, 683. <https://doi.org/10.3390/pr9040683>.
- Ergün, E.H.; Coşkun, S. Experimental Performance and Techno-Economic Analysis of an Air Conditioning System with an Ice Storage System. *Appl. Sci.* **2025**, *15*, 10088. <https://doi.org/10.3390/app151810088>.

12. Yang, T.; Liu, W.; Kramer, G.J.; Sun, Q. Seasonal thermal energy storage: A techno-economic literature review. *Renew. Sustain. Energy Rev.* **2021**, *139*, 110732. <https://doi.org/10.1016/j.rser.2021.110732>.
13. Mazzoni, S.; Sze, J.Y.; Nastasi, B.; Ooi, S.; Desideri, U.; Romagnoli, A. A techno-economic assessment on the adoption of latent heat thermal energy storage systems for district cooling optimal dispatch & operations. *Appl. Energy* **2021**, *289*, 116646. <https://doi.org/10.1016/j.apenergy.2021.116646>.
14. Hao, J.; Yang, Y.; Xu, C.; Du, X. A comprehensive review of planning, modeling, optimization, and control of distributed energy systems. *Carbon Neutrality* **2022**, *1*, 28. <https://doi.org/10.1007/s43979-022-00029-1>.
15. Guo, X.; Xu, X.; Wang, Z.; Chang, Z.; Chang, C. Research Progress on the Performance Enhancement Technology of Ice-on-Coil Energy Storage. *Energies* **2025**, *18*, 1734. <https://doi.org/10.3390/en18071734>.
16. Rahgozar, S.; Pourrajabian, A.; Dehghan, M. On the role of building use and operational strategy in integrating ice storage systems: An economic perspective. *J. Energy Storage* **2024**, *98*, 113025. <https://doi.org/10.1016/j.est.2024.113025>.
17. Lee, A.H.; Jones, J.W. Modeling of an ice-on-coil thermal energy storage system. *Energy Convers. Manag.* **1996**, *37*, 1493–1507. [https://doi.org/10.1016/0196-8904\(95\)00224-3](https://doi.org/10.1016/0196-8904(95)00224-3).
18. Bahmani, R.; Karimi, H.; Jadid, S. Cooperative energy management of multi-energy hub systems considering demand response programs and ice storage. *Int. J. Electr. Power Energy Syst.* **2021**, *130*, 106904. <https://doi.org/10.1016/j.ijepes.2021.106904>.
19. Chen, H.J.; Wang, D.W.; Chen, S.L. Optimization of an ice-storage air conditioning system using dynamic programming method. *Appl. Therm. Eng.* **2005**, *25*, 461–472. <https://doi.org/10.1016/j.applthermaleng.2003.12.006>.
20. Ma, T.; Wu, J.; Hao, L. Energy flow modeling and optimal operation analysis of the micro energy grid based on energy hub. *Energy Convers. Manag.* **2017**, *133*, 292–306. <https://doi.org/10.1016/j.enconman.2016.12.011>.
21. Allan, J.; Croce, L.; Dott, R.; Georges, G.; Heer, P. Calculating the heat loss coefficients for performance modelling of seasonal ice thermal storage. *J. Energy Storage* **2022**, *52*, 104528. <https://doi.org/10.1016/j.est.2022.104528>.
22. Goeke, J. Wärmeübertragung in Eisspeichern und Energiegewinne aus dem Erdreich. *Bauphysik* **2019**, *41*, 96–103. <https://doi.org/10.1002/bapi.201900001>. (In German)
23. Vivian, J.; Heer, P.; Fiorentini, M. Optimal sizing and operation of seasonal ice thermal storage systems. *Energy Build.* **2023**, *300*, 113633. <https://doi.org/10.1016/j.enbuild.2023.113633>.
24. Mancin, S.; Noro, M. Reversible Heat Pump Coupled with Ground Ice Storage for Annual Air Conditioning: An Energy Analysis. *Energies* **2020**, *13*, 6182. <https://doi.org/10.3390/en13236182>.
25. Tanino, M.; Kozawa, Y. Ice-water two-phase flow behavior in ice heat storage systems. *Int. J. Refrig.* **2001**, *24*, 639–651. [https://doi.org/10.1016/S0140-7007\(00\)00085-2](https://doi.org/10.1016/S0140-7007(00)00085-2).
26. Carbonell, D.; Philippen, D.; Haller, M.Y.; Brunold, S. Modeling of an ice storage buried in the ground for solar heating applications. Validations with one year of monitored data from a pilot plant. *Solar Energy* **2016**, *125*, 398–414. <https://doi.org/10.1016/j.solener.2015.12.009>.
27. Sevi, P.; Bernardin, F.; Cueur, A.; Stutz, B. Numerical and experimental study of an underground thermal energy storage system coupled with asphalt solar collector and heat pump. *J. Energy Storage* **2025**, *114*, 115769. <https://doi.org/10.1016/j.est.2025.115769>.
28. Candanedo, J.A.; Dehkordi, V.R.; Stylianou, M. Model-based predictive control of an ice storage device in a building cooling system. *Appl. Energy* **2013**, *111*, 1032–1045. <https://doi.org/10.1016/j.apenergy.2013.05.081>.
29. Zhao, J.; Liu, D.; Yuan, X.; Wang, P. Model predictive control for the ice-storage air-conditioning system coupled with multi-objective optimization. *Appl. Therm. Eng.* **2024**, *243*, 122595. <https://doi.org/10.1016/j.applthermaleng.2024.122595>.
30. Luo, N.; Hong, T.; Li, H.; Jia, R.; Weng, W. Data analytics and optimization of an ice-based energy storage system for commercial buildings. *Appl. Energy* **2017**, *204*, 459–475. <https://doi.org/10.1016/j.apenergy.2017.07.048>.
31. Thiem, S.; Born, A.; Danov, V.; Vandersickel, A.; Schäfer, J.; Hamacher, T. Automated identification of a complex storage model and hardware implementation of a model-predictive controller for a cooling system with ice storage. *Appl. Therm. Eng.* **2017**, *121*, 922–940. <https://doi.org/10.1016/j.applthermaleng.2017.04.149>.
32. Hao, L.; Wei, M.; Xu, F.; Yang, X.; Meng, J.; Song, P.; Min, Y. Study of operation strategies for integrating ice-storage district cooling systems into power dispatch for large-scale hydropower utilization. *Appl. Energy* **2020**, *261*, 114477. <https://doi.org/10.1016/j.apenergy.2019.114477>.
33. Vetterli, J.; Benz, M. Cost-optimal design of an ice-storage cooling system using mixed-integer linear programming techniques under various electricity tariff schemes. *Energy Build.* **2012**, *49*, 226–234. <https://doi.org/10.1016/j.enbuild.2012.02.012>.
34. Bschorer, S.; Kuschke, M.; Strunz, K. Object-oriented modeling for planning and control of multi-energy systems. *CSEE J. Power Energy Syst.* **2019**, *5*, 355–364. <https://doi.org/10.17775/CSEEJPES.2019.00650>.
35. Jia, L.; Liu, J.; Chong, A.; Dai, X. Deep learning and physics-based modeling for the optimization of ice-based thermal energy systems in cooling plants. *Appl. Energy* **2022**, *322*, 119443. <https://doi.org/10.1016/j.apenergy.2022.119443>.
36. Heine, K.; Tabares-Velasco, P.C.; Deru, M. Design and dispatch optimization of packaged ice storage systems within a connected community. *Appl. Energy* **2021**, *298*, 117147. <https://doi.org/10.1016/j.apenergy.2021.117147>.

37. Jalili, M.; Sedighizadeh, M.; Sheikhi Fini, A. Stochastic optimal operation of a microgrid based on energy hub including a solar-powered compressed air energy storage system and an ice storage conditioner. *J. Energy Storage* **2021**, *33*, 102089. <https://doi.org/10.1016/j.est.2020.102089>.
38. Heidari, A.; Mortazavi, S.S.; Bansal, R.C. Stochastic effects of ice storage on improvement of an energy hub optimal operation including demand response and renewable energies. *Appl. Energy* **2020**, *261*, 114393. <https://doi.org/10.1016/j.apenergy.2019.114393>.
39. Odufuwa, O.Y.; Kusakana, K.; Numbi, B.P.; Tartibu, L.K. Optimal energy management of grid-connected PV for HVAC cooling with ice thermal storage system. *J. Energy Storage* **2024**, *77*, 109844. <https://doi.org/10.1016/j.est.2023.109844>.
40. Sanaye, S.; Khakpaay, N. Thermo-economic multi-objective optimization of an innovative cascaded organic Rankine cycle heat recovery and power generation system integrated with gas engine and ice thermal energy storage. *J. Energy Storage* **2020**, *32*, 101697. <https://doi.org/10.1016/j.est.2020.101697>.
41. Dai, W.; Xia, W.; Li, B.; Goh, H.; Zhang, Z.; Wen, F.; Ding, C. Increase the integration of renewable energy using flexibility of source-network-load-storage in district cooling system. *J. Clean. Prod.* **2024**, *441*, 140682. <https://doi.org/10.1016/j.jclepro.2024.140682>.
42. Zheng, X.; Wu, G.; Qiu, Y.; Zhan, X.; Shah, N.; Li, N.; Zhao, Y. A MINLP multi-objective optimization model for operational planning of a case study CCHP system in urban China. *Appl. Energy* **2018**, *210*, 1126–1140. <https://doi.org/10.1016/j.apenergy.2017.06.038>.
43. Hoffmann, M.; Kotzur, L.; Stolten, D.; Robinius, M. A Review on Time Series Aggregation Methods for Energy System Models. *Energies* **2020**, *13*, 641. <https://doi.org/10.3390/en13030641>.
44. Kotzura, L.; Markewitz, P.; Robinius, M.; Stolten, D. Time series aggregation for energy system design: Modeling seasonal storage. *Appl. Energy* **2018**, *213*, 123–135. <https://doi.org/10.1016/j.apenergy.2018.01.023>.
45. Renaldi, R.; Friedrich, D. Multiple time grids in operational optimisation of energy systems with short- and long-term thermal energy storage. *Energy* **2017**, *133*, 784–795. <https://doi.org/10.1016/j.energy.2017.05.120>.
46. Gabrielli, P.; Gazzani, M.; Martelli, E.; Mazzotti, M. Optimal design of multi-energy systems with seasonal storage. *Appl. Energy* **2018**, *219*, 408–424. <https://doi.org/10.1016/j.apenergy.2017.05.152>.
47. Krien, U.; Schönfeldt, P.; Launer, J.; Hilpert, S.; Kaldemeyer, C.; Pleßmann, G. oemof.solph—A model generator for linear and mixed-integer linear optimisation of energy systems. *Softw. Impacts* **2020**, *6*, 100028. <https://doi.org/10.1016/j.simpa.2020.100028>.
48. Schönfeldt, P.; Schlütters, S.; Oltmanns, K. MTRESS 3.0—Modell Template for Residential Energy Supply Systems. *arXiv* **2022**, arXiv:2211.14080.
49. Schönfeldt, P.; Grimm, A.; Neupane, B.; Torio, H.; Duranp, P.; Klement, P.; Hanke, B.; von Maydell, K.; Agert, C. Simultaneous optimization of temperature and energy in linear energy system models. In Proceedings of the 2022 Open Source Modelling and Simulation of Energy Systems (OSMSES), Aachen, Germany, 4–5 April 2022; pp. 1–6. <https://doi.org/10.1109/OSMSES54027.2022.9768967>.
50. Viessmann Climate Solutions SE. Eis-Energiespeichersystem: Projektplanung für Vitocal Sole/Wasser-Wärmepumpen. 2022. Available online: <https://www.viessmann.de/de/produkte/waermepumpe/eis-energiespeicher-systeme-grossanlagen.html> (accessed on 13 November 2025). (In German)
51. West, J.; Braun, J.E. Modeling Partial Charging and Discharging of Area-Constrained Ice Storage Tanks. *HVAC&R Res.* **1999**, *5*, 209–228. <https://doi.org/10.1080/10789669.1999.10391234>.
52. Dohmann, J. *Thermodynamik der Kälteanlagen und Wärmepumpen*; Springer Vieweg: Berlin/Heidelberg, Germany, 2016. <https://doi.org/10.1007/978-3-662-49110-2>. (In German)
53. Castell, A.; Belusko, M.; Bruno, F.; Cabeza, L.F. Maximisation of heat transfer in a coil in tank PCM cold storage system. *Appl. Energy* **2011**, *88*, 4120–4127. <https://doi.org/10.1016/j.apenergy.2011.03.046>.
54. Krien, U.; Kaldemeyer, C.; Günther, S.; Schönfeldt, P.; Simon, H.; Launer, J.; Röder, J.; Möller, C.; Kochems, J.; Huyskens, H.; et al. oemof.solph (v0.5.2), 2024. <https://doi.org/10.5281/zenodo.10497413>.

Disclaimer/Publisher’s Note: The statements, opinions and data contained in all publications are solely those of the individual author(s) and contributor(s) and not of MDPI and/or the editor(s). MDPI and/or the editor(s) disclaim responsibility for any injury to people or property resulting from any ideas, methods, instructions or products referred to in the content.